The global pattern of evolution of plasmaspheric drainage plumes

J. Goldstein

Space Science and Engineering Division, Southwest Research Institute, San Antonio, TX 78228 USA

B. R. Sandel

Lunar and Planetary Laboratory, University of Arizona, Tucson, AZ 85721 USA

We present observations of an 18 June 2001 erosion event obtained by the IMAGE extreme ultraviolet (EUV) imager. Following a 0304 UT southward turning of the interplanetary magnetic field (IMF), the plasmasphere on both nightside and dayside surged sunward, reducing the plasmasphere radius on the nightside and creating a broad drainage plume on the dayside. Over several hours this plume narrowed in magnetic local time (MLT), until shortly after a northward IMF turning between 1430 UT and 1500 UT, when the plume began corotating with the Earth. On a global scale, the 18 June EUV plasmasphere observations are consistent with the interpretation that dayside magnetopause reconnection (DMR) during southward IMF produced a sunward convection field in the inner magnetosphere. Using the Volland-Stern electric potential model normalized to the solar wind E-field, we performed a simple plasmapause test particle (PTP) simulation of the 18 June event and found good global agreement with EUV observations, but important sub-global differences as well. On a sub-global scale, proper treatment of plasmaspheric dynamics requires consideration of sub-auroral polarization streams (SAPS) and penetration electric field to explain narrow duskside plumes and preferential pre-dawn plasmapause motion, respectively. The 18 June 2001 EUV images contain evidence of a double plume (or bifurcation of a single plume) and dayside crenulations of the plasmapause, both of which remain unexplained. The observations suggest that strong convection suppresses or smooths plasmapause structure, which tends to increase during times of weak or absent convection. Analysis of the motion of the plasmapause on 18 June 2001 reveals some of the details of the initial erosion process, which apparently involves partial indentation of the plasmapause and subsequent widening of this indentation to other MLT sectors eastward and westward of the initial indentation, and produces 'rotated V' signatures in the electric field. Early erosion on 18 June was bursty, and modulated by the solar wind electric field; convection was turned on during southward IMF and turned off during northward IMF. Northward IMF apparently triggered overshielding, causing the formation of a midnight-to-dawn plasmapause bulge that subsequently corotated. It is clear that more detailed information about the inner magnetospheric E-field is required to fully understand plasmaspheric dynamics.

1. Introduction

1.1. Dayside Magnetopause Reconnection (DMR), Erosion, and Plume Formation

It is widely accepted that when the IMF turns southward, reconnecting field lines are dragged antisunward, driving magnetospheric convection in which the outer magnetospheric plasma moves tailward and inner magnetospheric plasma moves sunward [*Dungey*, 1961]. The strength of this dayside magnetopause reconnection (DMR) driven convection should fluctuate in time in accord with variations in the solar wind (SW) and interplanetary magnetic field (IMF). The main influence seems to be the polarity of the Z-component $B_{Z,\mathrm{IMF}}$ of the IMF. During southward IMF (negative $B_{Z,\mathrm{IMF}}$) DMR drives convection; during northward IMF ($B_{Z,\mathrm{IMF}} > 0$) DMR convection shuts off. Numerous studies (e.g., see *Carpenter et al.* [1993]; *Carpenter* [1995]; *Carpenter and Lemaire* [1997]; *Lemaire and Gringauz* [1998], and many observational and theoretical papers referenced therein) have shown that the strength of DMR-driven sunward convection is a primary influence on the dynamics and structure of the plasmasphere, the cold, rotating torus of plasma that surrounds the Earth and (on average) extends to equatorial distances of 4–6 earth radii (R_{E}). A strong change in DMR-driven convection can cause the outer boundary of the plasmasphere, the plasmapause, to move either radially inward (compression) or outward (rarefaction). A DMR convection increase may also produce an azimuthal plasma motion in which the outer layer of the plasmasphere is stripped away, a process known as plasmaspheric erosion. The hypothetical DMR-driven convection offers an explanation for why the plasmasphere shrinks during increased geomagnetic activity [*Chappell et al.*, 1970a], and why in situ observations imply the presence of a bulge near dusk [*Chappell et al.*, 1970b; *Higel and Wu*, 1984].

The details of the erosion process are not yet completely understood [*Carpenter and Lemaire*, 1997], but one known byproduct of erosion is the drainage plume. Plumes (also called 'tails') are regions of plasmaspheric plasma that are connected to the main body of the plasmasphere and extend outward into the surrounding tenuous plasma. Plumes were predicted on the basis of theoretical models of the effects of increases in DMR-driven convection [*Grebowsky*, 1970; *Chen and Wolf*, 1972; *Spiro et al.*, 1981; *Elphic et al.*, 1996; *Weiss et al.*, 1997; *Lambour et al.*, 1997]. In situ observations of outlying or 'detached' plasma, separated from the main plasmasphere [*Chappell*, 1974; *Carpenter and Anderson*, 1992], seemed consistent with the plume interpretation. An alternate explanation, that the de-

tached plasma was due to 'blobs' completely separated from the plasmasphere, was offered by *Chappell* [1974], and the mechanism for creation of blobs by gravitational/centrifugal interchange instability was proposed by *Lemaire* [1975].

The existence of plumes of high-density plasmaspheric material has been conclusively demonstrated by global plasmaspheric images [*Sandel et al.*, 2001; *Burch et al.*, 2001; *Foster et al.*, 2002; *Goldstein et al.*, 2002, 2003a; *Spasojević et al.*, 2003; *Goldstein et al.*, 2003c, b, 2004b; *Sandel et al.*, 2003]. It should be noted that the global plasmaspheric images do not see the complete plasma distribution, but rather only the high-density portion, corresponding to total number densities above about 40 cm^{-3} [*Goldstein et al.*, 2003c; *Moldwin et al.*, 2003]. It is for this reason that we say 'plumes of high-density plasmaspheric material.' At densities below 40 cm^{-3}, completely detached blobs of plasma may indeed exist but still be invisible in plasmaspheric images. Plasmasphere images show there is a strong correlation between $B_{Z,\mathrm{IMF}}$ polarity and the behavior of the plasmasphere during both southward [*Goldstein et al.*, 2003a; *Spasojević et al.*, 2003] and northward [*Goldstein et al.*, 2002, 2003d] IMF polarities. From plasmaspheric imaging, the formation and subsequent evolution of plasmaspheric plumes follows a predictable pattern that depends primarily on IMF polarity, as follows.

1.1.1. Sunward Surge Following an increase in the magnitude of southward IMF, the plasmaspheric plasma surges sunward. On the nightside the plasmapause radius decreases (moves sunward/earthward), and on the dayside the plasmapause location increases (moves sunward). The increased extent of the dayside plasmasphere forms a plume that is broad in magnetic local time (MLT) extent, and which extends outward in the $+X$-direction.

1.1.2. Plume Narrowing If the IMF polarity remains southward at its surge-time level for several hours, the plume formed during the initial sunward surge then undergoes a period of narrowing, in which the the dusk edge of the plume remains relatively stationary while the western edge of the plume slowly rotates eastward. Models provide some information about plume narrowing. The plume forms following an enhancement in convection, and concomitant inward motion of the corotation/convection boundary (CCB), and as time advances and the erosion progresses, less plasmaspheric material remains outside the CCB to 'feed' the plume, causing it to narrow. Also, the innermost western edge of the plume may lie within the CCB and thus tends to rotate with the Earth, while the dusk edge tends to

line up with the CCB and thus is roughly stationary during steady convection. Models also suggest that if this plume narrowing phase continues indefinitely, the western edge eventually reaches the dusk edge, and the plume disappears/dissipates.

1.1.3. Plume Rotation/Wrapping   Eventually, the IMF turns northward, and in EUV images the narrowed plume begins to rotate eastward and wrap about the main plasmasphere. The DMR convection hypothesis explains this plume rotation as follows. When the IMF turns northward, the CCB expands to larger radial distances, and the plume that was formerly in the convection zone is now in the corotation regime and thus begins to rotate. Inside the CCB, the rotation rate decreases with distance from the Earth on the dusk side, and this flow shear distorts the shape of the plume. The base of the plume (near the plasmasphere) moves faster than the end of the plume, so the plume lengthens as it rotates. If quiet conditions prevail long enough, the plume rotates until it encounters the new location of the CCB, and then it lengthens and wraps around the plasmasphere. *Spasojević et al.* [2003] showed a particularly dramatic example of this rotation/wrapping process that occurred on 10–11 June 2001.

The EUV-observed phases of plume evolution (sunward surge, plume narrowing, and plume rotation/wrapping) are entirely consistent with (and indeed were predicted by) model plasmaspheres subject to DMR-driven convection (e.g., *Grebowsky* [1970]; *Spiro et al.* [1981]), and also agree with prior in situ observations [*Elphic et al.*, 1996]. The eastward rotation of the plume during northward IMF is also in accord with in situ observations of the rotating duskside bulge [*Higel and Wu*, 1984; *Moldwin et al.*, 1994].

1.2. Details of the Erosion Process

Although the zero-order (i.e., global) active-time plasmaspheric dynamics are adequately described by the phases of plume evolution and the DMR-driven convection hypothesis, this simple picture is clearly incomplete.

There remain important questions about the mechanisms involved in transferring SW/IMF energy to the inner magnetosphere. The first question is, how is that energy transferred? *Goldstein et al.* [2003a] noted that there is a time delay (which they dubbed 'configuration delay' $\Delta\tau_C$) between the arrival of southward IMF at the magnetopause and the subsequent inward motion of the nightside plasmapause. This time delay $\Delta\tau_C$ has so far been consistently observed (in plasmasphere images) to be between 20 and 30 minutes when reasonably

precise timing of the SW and IMF arrival at the magnetopause was available [*Spasojević et al.*, 2003; *Goldstein et al.*, 2003a, b, 2004b]. The cause of the delay $\Delta\tau_C$ is perhaps explainable as the time necessary for the entire magnetospheric DMR convection field to reconfigure following a southward IMF turning [*Coroniti and Kennel*, 1973]. This reconfiguration explanation has yet to be conclusively established, and the details of the reconfiguration process, surely involving coupled interactions of the ionosphere, plasmasheet, and ring current, remain unknown. Another question is, how much of the SW/IMF energy is transmitted to the inner magnetosphere? It is known that the inner magnetosphere inside the plasmasheet is to some (time-varying) degree shielded from DMR driven convection [*Jaggi and Wolf*, 1973]. However, effective shielding probably requires between 15 minutes and 1 hour to develop [*Kelley et al.*, 1979; *Senior and Blanc*, 1984; *Goldstein et al.*, 2003d], so that it probably cannot respond to more rapid changes in DMR-driven convection driven by the ever-present fluctuations in the SW and IMF. Thus, under quickly varying geomagnetic conditions the external convection field can 'penetrate' past the shielding layer. This so-called penetration E-field has been observed in ionospheric and equatorial in situ measurements [*Fejer et al.*, 1990; *Fejer and Scherliess*, 1995; *Scherliess and Fejer*, 1997; *Wygant et al.*, 1998], and there are indications that it can be 'focused' into the midnight-to-dawn MLT sector. From analysis and modeling of global plasmasphere images, *Goldstein et al.* [2003b, 2004c] estimated that between 12 and 25 percent of the solar wind E-field can be transmitted to the inner magnetosphere during plasmasphere erosion events.

A question of continuing interest (and at times, mild controversy) is: how and where does plasma redistribute itself to form a new plasmapause boundary, particularly during erosion? According to the DMR-driven convection hypothesis, when the plasmapause boundary moves inward (as it does on the nightside during erosion events), the plasma at the boundary moves both radially inward and azimuthally (either eastward or westward, depending on the MLT sector), and the net effect is a reduction of the plasmapause radius [*Grebowsky*, 1970; *Spiro et al.*, 1981]. However, the possible role of plasma instabilities in the erosion process is unknown. According to proponents of the gravitational/centrifugal interchange hypothesis [*Lemaire*, 1975; *Lemaire and Gringauz*, 1998], during erosion (i.e., inward radial plasmapause motion) the nightside plasma actually moves radially outward, forming detached blobs that might show up as fine-scale den-

sity structure outside the main plasmapause [*LeDocq et al.*, 1994; *Moldwin et al.*, 1995]. Possibly related to this topic is the unresolved issue of quiet-time plasmaspheric density structure. During or following extended quiet periods, the plasmasphere exhibits a great deal of as-yet unexplained meso-scale and fine-scale structure in the form of 'blobby' density regions, irregular plasmapause shapes, fingerlike density enhancements, and isolated high-density flux tubes found in the interior of the plasmasphere [*Moldwin et al.*, 1994, 1995, 2003; *Sandel et al.*, 2001; *Spasojević et al.*, 2003; *Dent et al.*, 2003; *Goldstein et al.*, 2004b]. What causes these density structures? One explanation is that the interchange instability, which during active times is suppressed by ring current pressure and/or high ionospheric conductivity [*Richmond*, 1973; *Huang et al.*, 1990], might during quiet times have a significant effect on plasmaspheric structure. It has also been suggested that during quiet times, in the absence of strong forcing by dayside reconnection, the inner magnetospheric electric field becomes disorganized and spatially structured, creating the observed quiet-time density characteristics [*Moldwin et al.*, 1994].

A significant modification of DMR-driven convection is the subauroral polarization stream (SAPS). SAPS– also known as subauroral ion drifts (SAID) or polarization jets–are a disturbance-time effect in which feedback between the ring current and ionosphere produces an intense, radially narrow, westward flow channel in the dusk-to-midnight MLT sector [*Foster and Burke*, 2002; *Foster et al.*, 2002; *Foster and Vo*, 2002; *Anderson et al.*, 2001; *Burke et al.*, 1998, 2000]. Ionospheric SAPS occur when the equatorward boundaries of the ion and electron precipitation separate, leading to a poleward Pedersen current in the subauroral ionosphere, connected to the the ion and electron plasmasheets via region 2 and region 1 field aligned currents, respectively. Due to the low conductivity at subauroral latitudes, the poleward Pedersen current generates intense poleward E-fields that are then mapped to the equatorial plane as radial E-fields confined between the inner edges of the ion and electron plasmasheets. Thus, SAPS form a radially-narrow (1 to 2 $R_{\rm E}$) flow channel bordering or overlapping the dusk-to-midnight plasmasphere. Because of the ring-current/ionosphere feedback involved in SAPS generation, the magnetopause IMF polarity does not directly turn SAPS on and off as it does DMR convection; SAPS can persist even when DMR-driven convection has subsided following a northward IMF turning. SAPS have been demonstrated to modify plasmasphere dynamics in the dusk-to-midnight MLT sector by inten-

sifying sunward convection, which sharpens the outer radial density gradient at the plasmapause boundary, smooths the MLT shape of the plasmapause, and at times creates narrow duskside plumes that are distinct from the broad dayside DMR-driven Grebowsky plumes [*Foster et al.*, 2002; *Goldstein et al.*, 2003b, 2004b, a].

1.3. 18 June 2001: Start-to-Finish Plume Evolution

In this paper we present global images of the plasmasphere obtained on 18 June 2001, when a plasmasphere erosion occurred following a southward IMF turning early in the day. We will examine these observations in the context of the hypothesis that dayside magnetopause reconnection (DMR) drives convection that exerts a primary global influence on the plasmasphere. The 18 June 2001 event exemplifies the pattern of plume evolution implied by the models of *Grebowsky* [1970] and others, and observed in part during other erosion events (e.g., *Elphic et al.* [1996], *Spasojević et al.* [2003], *Goldstein et al.* [2004b]). The appeal of this event is that global imaging observations were available to witness all the phases of plume evolution (sunward surge, plume narrowing, and plume rotation/wrapping), providing excellent coverage (with the exception of a data gap during the plume narrowing phase) of the plume formation and evolution from start to finish. By studying this single start-to-finish event, we can observe the creation and subsequent evolution of particular features of the plasma distribution, and more clearly identify ways in which the plasmasphere behaves both according to, and in disagreement with, the simple DMR-driven convection picture.

2. Observations 18 June 2001

In this section we present solar wind and interplanetary magnetic field (IMF) data, and global plasmasphere observations, during a plasmasphere erosion event that occurred on 18 June 2001. On this day, the overall geomagnetic conditions were those of a weak-to-moderate magnetic storm. The storm sudden commencement occurred between 0300 UT and 0400 UT, and Dst reached a minimum of -61 nT between 0900 UT and 1000 UT.

2.1. Solar Wind and IMF

On 18 June 2001 the Advanced Composition Explorer (ACE) spacecraft [*Stone et al.*, 1998] was located approximately 244 R_E upstream of the Earth, and about 32 R_E duskward of the Earth-Sun line. Figure 1 shows data from the MAG [*Smith et al.*, 1998] and SWEPAM [*McComas et al.*, 1998] instruments. The ACE data

Figure 1

have been propagated to the magnetopause by adding a time delay of 60 ± 10 minutes, calculated as V_{SW}/X. The uncertainty ± 10 minutes in our propagation delay is for this event slightly larger than that of other published erosion events (e.g., *Goldstein et al.* [2003a]). The imprecise timing of the arrival of the solar wind at the magnetopause will affect the reliability of our estimate of $\Delta\tau_{\mathrm{C}}$, the configuration delay for the 18 June 2001 event (see Section 2.2.2).

Figure 1a and Figure 1b plot the IMF polarity $B_{Z,\mathrm{IMF}}$ and solar wind speed V_{SW}, respectively. At about 0300 UT a mild shock/transition arrived at the magnetopause, bringing a $+60$ km/s step-like increase in V_{SW} at 0257 UT and a somewhat noisy excursion from mild southward IMF ($B_{Z,\mathrm{IMF}} \geq -3$ nT) to strong southward IMF ($B_{Z,\mathrm{IMF}} \leq -10$ nT) at 0304 UT. According to the DMR-driven convection hypothesis, this southward IMF excursion should impose on the magnetosphere a duskward solar wind electric field (corresponding to sunward $E \times B$ convection). Figure 1c plots the dawnward solar wind E-field ϵ_{SW}, defined as $\epsilon_{\mathrm{SW}} \equiv V_{\mathrm{SW}}B_{Z,\mathrm{IMF}}$ so that ϵ_{SW} is negative when the IMF is southward. Therefore, in this paper we will use the terms 'negative ϵ_{SW}' and 'southward IMF' somewhat interchangeably. From the results of *Goldstein et al.* [2003a, b], we expect some delay $\Delta\tau_{\mathrm{C}}$ between the IMF and the effects of ϵ_{SW} on the plasmasphere, so we have delayed ϵ_{SW} by $\Delta\tau_{\mathrm{C}} = 10$ minutes (as indicated in Figure 1c). (Determination of the value of $\Delta\tau_{\mathrm{C}}$ for this event is discussed later, in Section 2.2.2). Because the DMR-driven E-field forms the conceptual framework of this paper, the plot of ϵ_{SW} in Figure 1c will be repeated to aid discussion of Plate 1 and Plate 3.

In the next section we present plasmasphere images obtained by the IMAGE EUV instrument.

2.2. Global Plasmasphere Images

The extreme ultraviolet (EUV) instrument on the IMAGE satellite is an imaging system composed of three cameras (with slightly overlapping fields of view) sensitive to the 30.4-nm ultraviolet light that is resonantly scattered by the He$^+$ ions in the plasmasphere [*Burch*, 2000; *Sandel et al.*, 2000, 2001]. IMAGE EUV sees the He$^+$ portion of the plasmasphere corresponding to total number densities above about 40 cm^{-3} [*Goldstein et al.*, 2003c; *Moldwin et al.*, 2003]. On 18 June 200 the IMAGE satellite was in a roughly dawn-dusk orbit, with its 8.2 R_{E} apogee almost directly over the north magnetic pole. This apogee location provided an excellent viewing geometry, with minimal sunlight

contamination and perspective distortion in the images, and a wide field of view that most of the time extended to or beyond geosynchronous orbit.

Plate 1 shows 12 panels of EUV image data, labeled a, b, c, ..., j, k, l and arranged in 3 rows of 4 panels each, depicting a sequence of plasmapause images from 0010 UT through 1854 UT. In the figure, time increases from left to right in each row, and from top to bottom between rows, as indicated by the UT stamps at the bottom of the panels. Each panel shows the equatorial distribution of line-of-sight integrated He$^+$ column abundance. These equatorial maps were obtained using the procedure outlined in *Dent et al.* [2003] and *Goldstein et al.* [2004b]. Color indicates column abundance (in arbitrary units), increasing from black (zero) to white (very dense plasma). The plasmasphere is the green/white region surrounding the Earth. In each image, the plasmapause is the (often sharp) dropoff in signal intensity which occurs (on average in Plate 1) between $L = 2.5$ and $L = 4$. (For the reader unfamiliar with identification of the plasmapause in EUV images, see *Goldstein et al.* [2003c] and the plasmapause extractions of the bottom row of Plate 2.) Outside the plasmapause, the dark green speckled background represents plasma total number densities at or below the EUV lower noise floor (i.e., ≤ 40 cm^{-3}). The EUV field of view (FOV) edges vary as IMAGE progresses through its orbit. The FOV edges (labeled for demonstrative purpose in Plate 1d) are the black regions that may cut across the plasmasphere near the borders of the images.

To provide context for the 12 EUV images, the bottom panel of Plate 1 shows ϵ_{SW} (from Figure 1c). For reference, the times of the 12 EUV snapshots of Plate 1a through Plate 1l are shown as labeled vertical lines in the ϵ_{SW} plot. The solar wind E-field ϵ_{SW} is defined so that its sign (positive or negative) indicates IMF polarity (northward or southward). We plot ϵ_{SW} instead of $B_{Z,IMF}$ because (1) we wish to emphasize the finite delay $\Delta\tau_C$ between southward IMF at the magnetopause and its effect on the inner magnetosphere, and (2) it is the electric field that directly drives convection of cold $E \times B$-drifting plasma in the inner magnetosphere. Said another way, we wish to distinguish the effect (the E-field that drives plasma convection) from the cause (dayside magnetopause reconnection). Negative ϵ_{SW} means there is a dawn-to-dusk E-field, or sunward convection in the inner magnetosphere.

The 18 June 2001 EUV images of Plate 1 quite fortunately capture the plasmasphere for some finite time during each of the phases of plume evolution during a single erosion event. We will first discuss the overall

Plate 1

global plasma behavior, and how it compares to the DMR-driven convection hypothesis.

2.2.1. Initial Plasmasphere Plate 1a shows the plasmasphere at 0010 UT, at the start of the event. At that time, the plasmasphere was radially large and irregularly shaped, with a large ($L \approx 5$) bulge centered at noon MLT, and notches (i.e., regions of decreased plasmapause radius) at 1100 MLT and between 1600 MLT and 1800 MLT. The outer edge of the dayside plasmasphere was diffuse, representing gradual/gentle outer density gradients. Outside these bulges and notches on the dayside, green speckling indicates some small amount of outlying plasma whose density was just above or at the EUV noise floor. In the image, the outer edge of the plasmasphere between 1800 MLT and 2100 MLT, and between 0600 MLT and 1100 MLT contains noisy brightness fluctuations that indicate spatial structure on scales below 0.5 R_{E}. Shape irregularity, diffuse boundaries, low-density outlying plasma, and spatial structure are characteristics typically found in quiet-time plasmasphere images [*Sandel et al.*, 2001; *Goldstein et al.*, 2003b]. On the other hand, in the nightside range 2100 MLT to 0600 MLT the plasmapause was relatively smooth and sharp, with little or no indication of outlying low-density plasma; this is typical of active time plasmasphere images. From the ϵ_{SW} plot in Plate 1, at 0010 UT the dawn-to-dusk solar wind E-field was well under 1 mV/m (which, according to the transmission factors of *Goldstein et al.* [2003b, 2004c] corresponds to 0.1–0.25 mV/m near the plasmasphere); i.e., at this time there was very weak but finite sunward convection and this weak convection had prevailed since 1600 UT of the previous day. So the dayside plasmasphere of Plate 1a reflects the relatively quiet conditions (presumably accompanied by dayside ionospheric filling of plasmaspheric flux tubes) that preceded 0010 UT, but the nightside reflects the mild convection that only had the ability to affect the local time range 2100 MLT to 0600 MLT. The DMR convection hypothesis has nothing to say about ionospheric filling of the plasmasphere, but the smooth plasmapause shape on the nightside is entirely consistent with the idea that mild sunward convection was in effect. After relatively steady convection for several hours, the DMR picture says the plasmapause location coincides approximately with the corotation/convection boundary (CCB), which was probably the case for the 0010 UT plasmapause between 2100 MLT and 0600 MLT. The 0010 UT plasmasphere illustrates how the plasmapause location and shape at different MLTs can arise due to a combination of accumulated effects and direct driving by the solar wind

and IMF. Between 0010 UT and about 0314 UT the dayside bulges and notches corotated with the Earth, while the nightside smooth plasmapause remained almost perfectly stationary.

2.2.2. Sunward Surge: Plume Formation On 18 June 2001 erosion commenced at some time between 0304 UT and 0324 UT. Unfortunately, the EUV images during the interval 0243–0324 UT contained an excessive amount of background noise, making interpretation very difficult, but not impossible. (Background noise in EUV images is believed to arise due to direct energetic particle excitation.) Our best guess is that the erosion started at 0314 UT (with an uncertainty of ± 10 minutes due to the noise-related ambiguity in EUV images). In Plate 1, panels b, c, and d depict the initial phase of the 18 June erosion. The nightside plasmasphere contracted, moving 1–1.5 R_E inward in about 4 hours of UT. The dayside plasma surged sunward, forming a broad (in MLT) drainage plume. To illustrate the dayside sunward surge, compare Plate 1a (0010 UT) and Plate 1d (0659 UT). The noon MLT bulge of Plate 1a expanded sunward (in an apparent plasma rarefaction) to form the plume of Plate 1d, which extended outside the camera field of view (FOV). The simultaneous inward nightside motion and outward dayside motion is exactly the global behavior predicted by the DMR convection hypothesis. In this picture, the 0304 UT southward IMF excursion (Figure 1a) turned on dayside magnetopause reconnection, and at 0314 UT the effect of this DMR was felt as an enhanced dawn-to-dusk convection E-field at the plasmasphere, which initiated the sunward surge and plume formation. This suggests a configuration delay $\Delta \tau_C$ of 10 minutes, which is significantly shorter than the 20–30-minute delays reported in previous EUV-observed erosion events [*Goldstein et al.*, 2003a, b]. However, ± 10-minute uncertainty in both the ACE propagation delay (Section 2.1) and the EUV erosion onset timing (above) yields 200 percent uncertainty in $\Delta \tau_C$. Despite this timing ambiguity, the global evolution is consistent with the DMR convection picture. Note in Plate 1d how exceptionally sharp the plasmapause radial gradient is, and how smooth its MLT shape is on the nightside, especially east of 2100 MLT. This 0659 UT snapshot was obtained following a 1-hour interval of strong, steady solar wind E-field ϵ_{SW} (see bottom panel of Plate 1). The DMR picture says steady convection should produce a corotation/convection boundary (CCB) that is very stable in time, leading to a sharp nightside plasmapause gradient that coincides roughly with the CCB.

In Section 2.2.5 we will discuss some meso-scale fea-

tures of the sunward surge plasmasphere (a narrow duskside plume and a predawn indentation) that suggest a more spatially structured inner magnetospheric flow field than is typically assumed in the simple global DMR-driven convection picture.

2.2.3. Plume Narrowing Between 0709 UT and 1205 UT there are no EUV images available. (EUV turns off when close to the magnetic equator, and during perigee.) During this time, the dawnward solar wind E-field ϵ_{SW} was strong and fairly steady at an average value of $\epsilon_{\mathrm{SW}} = -4$ mV/m (i.e., dawn-to-dusk E-field, sunward convection). Under DMR convection this should have resulted in a gradual narrowing of the broad dayside (sunward surge) plume, as the western edge of the plume rotated eastward toward the relatively stationary dusk edge of the plume. The plasmasphere of 0659 UT (Plate 1d) had a plume whose western edge was at about 0700 MLT, judging from the intersection of the plume with the FOV edge at about $L = 3.5$. Five hours later, at 1215 UT (Plate 1e), the western edge of the same plume crossed $L = 4$ at about 1200 MLT. This is clear evidence that the plume narrowing process did indeed occur during the five-hour gap in EUV data coverage.

Between 1215 UT and 1418 UT (the UT interval covered by the image sequence in panels e through g of Plate 1), ϵ_{SW} underwent slow, 3–4-mV/m peak-to-peak oscillations, presumably turning DMR convection on and off, and after about 1430 UT the IMF turned northward (ϵ_{SW} positive). Thus, the images in panels e, f, and g of Plate 1 were obtained at the tail end of the plume narrowing process; most of the plume narrowing had already occurred during the five-hour EUV data gap. Still, the western edge of the plume at 1418 UT was 1 to 1.5 MLT hours eastward of its location at 1215 UT, so this process continued until DMR convection turned off at 1430 UT.

As in the sunward surge phase, the EUV images of the plume narrowing phase contain sub-global density structures (a plume bifurcation and post-dawn crenulations) that will be discussed in Section 2.2.5.

2.2.4. Plume Rotating/Wrapping At 1430 UT the IMF began a slow northward turning, as reflected in the ϵ_{SW} transition from -3 mV/m at 1430 UT to 2 mV/m at 1500 UT. Between 1500 UT and 1830 UT ϵ_{SW} had a mean value of about $+1$ mV/m, corresponding to northward IMF and much-reduced sunward convection. In response, the entire plume began rotating eastward, evident in the images of Plate 1, panels h through l. After 1712 UT (Plate 1k) the plume shape became distorted, lengthening as it just barely began the process of wrap-

ping around the plasmasphere before EUV image coverage stopped.

The post-1500 UT interval of northward IMF saw outward radial motion of the plasmapause. Between 1509 UT (Plate 1i) and 1854 UT (Plate 1l) the post-midnight plasmapause moved outward by almost a full R_E. Part of this outward plasmapause motion may arise from rotation of the entire plasmasphere inside the CCB; since the nightside plasmapause radius increased in the westward direction, eastward rotation of the entire plasmasphere would result in an outward motion of the plasmapause at a fixed MLT value. However, analysis of the motion of the plasmapause during this time (see Section 2.3.3) suggests that this rotation scenario is an insufficient explanation.

Fine-scale and meso-scale structure in the EUV images of the plume rotation phase will be discussed in the next section.

2.2.5. Sub-Global Plasma Structures In Sections 2.2.2 through 2.2.4 we showed to what extent the IMAGE EUV observations of the 18 June 2001 erosion event conformed to the global picture of plasmasphere evolution according to the simple DMR-driven convection picture. In this section we shall examine some sub-global (meso-scale and fine-scale) plasmaspheric density features from this event.

Plate 2 shows four selected snapshots from the event (with their corresponding panel letters from Plate 1), labeled according to the plume evolution phases: 'Initial' (Plate 2a), 'Sunward Surge' (Plate 2c), 'Plume Narrowing' (Plate 2g), and 'Plume Rotating' (Plate 2k). In each panel of the bottom row of Plate 2 is a plot of points (blue circles) that have been manually extracted from the EUV image directly above it. These extracted points do not necessarily follow contours of brightness, but rather are intended to highlight certain components of the EUV images that may not be obvious to the reader who is unfamiliar with EUV image interpretation.

The EUV images show some indirect evidence of a pre-dawn concentration of the effects of convection. During the sunward surge phase, the plasmapause is preferentially indented in pre-dawn MLT. Evidence of this can be seen in the 'flattening' of the 0537 UT plasmapause (Plate 1c, Plate 2c) between about 0300 MLT and 0500 MLT, and in the smooth indentation of the 0659 UT plasmapause (Plate 1d) between 0400 MLT and 0600 MLT. It is possible that this reflects a 'focusing' of the convection field in the pre-dawn MLT sector that has been identified in both models and observations [*Carpenter et al.*, 1972, 1993; *Carpenter and*

Plate 2

Smith, 2000; *Senior and Blanc*, 1984; *Fejer and Scherliess*, 1995].

There is evidence of the presence of SAPS during the sunward surge phase, in the form of a narrow duskside plume (labeled in Plate 2c) that is separated from the main Grebowsky-type plume by a narrow density channel. In a comparison between EUV images and simulations, *Goldstein et al.* [2003b] showed how SAPS can create just such a distinct narrow plume. On 18 June, this duskside plume seemed to evolve from a sunward stretching of the duskside bulge whose western edge was at 1700–1800 MLT in the initial plasmasphere of 0010 UT (Plate 2a). Even though the initial erosion began at 0314 UT, the duskside bulge did not fully develop into a plume until about 0500 UT, when DMSP drift meter data show the early development of a mild SAPS event that continued throughout much of the day and peaked between 0900 UT and 1100 UT [http://cindispace.utdallas.edu/DMSP/, data not shown]. Preliminary examination of LANL MPA particle and flow data also support the presence of SAPS at this time [M. Thomsen, 2003, private communication]. After 0500 UT, the dusk edge of the plume also achieved a steeper, more definite density gradient, as well as a smoother MLT shape; this is also in agreement with the observed and modeled effects of SAPS on the duskside [*Foster et al.*, 2002; *Goldstein et al.*, 2003b, 2004b].

There is also indirect evidence of the presence of SAPS during the plume narrowing phase. From Plate 1, plume narrowing occurred roughly between 0600 UT and 1430 UT, and during this time the dusk edge was relatively stationary. In the DMR convection picture the dusk edge of the plume moves eastward or westward in response to corresponding expansion or contraction of the CCB. Considering the relatively steady ($\epsilon_{\mathrm{SW}} \approx -4$ mV/m) conditions between 0600 UT and 1200 UT, it is not surprising that the dusk edge did not move much during the five-hour EUV data gap. What is perhaps in conflict with the DMR-driven convection picture is that the dusk edge also did not move during the 3–4-mV/m peak-to-peak ϵ_{SW} oscillations between 1200 UT and 1430 UT. In Section 3 we will use a simple DMR-based simulation to show that the oscillation in ϵ_{SW} produces a very mild, 0.4 R_{E} translation of the Y location of the dusk edge of the plume. There was also during this period some mild SAPS activity in DMSP ionospheric data [http://cindispace.utdallas.edu/DMSP/, data not shown]; it is perhaps plausible that mild SAPS could stabilize the small motion of the dusk edge of the plume, provided that the SAPS flow intensity was rela-

tively insensitive to changes in dayside magnetopause reconnection (DMR). SAPS form due to an internal coupling process that is distinct from DMR so although SAPS are often affected by DMR, it is conceivable that SAPS might exist even when DMR-driven convection is weak, or that SAPS could be maintained at a relatively constant intensity during fluctuating DMR-driven convection such as during 1200 to 1430 UT. This hypothesis deserves investigation in future studies.

One notable feature of the EUV data after 1215 UT is that the plume was bifurcated by a shallow low density channel, forming a 'double-plume' in the noon-to-dusk MLT sector, as depicted in Plate 2g. This double plume survived into the plume rotation phase after 1500 MLT (see 1712 UT plasmasphere of Plate 2k). Because of the EUV data gap between 0709–1205 UT we can only speculate on the origin of the double plume. Although not prohibited by the DMR convection picture, the formation of the double plume seems to require either (1) a more highly structured noon-to-dusk electric field than is customarily included in DMR-driven convection models; or (2) density variations one or two MLT hours wide, contained within the dayside plasmasphere distribution, that gradually evolved or were distorted/elongated by sunward convection. It is reasonable to wonder if the double plume arose somehow through a distortion of the earlier narrow duskside plume and the broad dayside plume (Plate 2c), but this seems unlikely. Notice from Plate 1d that by 0659 UT the duskside plume was extremely narrow and seemed to merge into the dusk edge of the main dayside plume. In order for this very narrow 0659 UT duskside plume to later evolve into the wider dusk portion of the double plume, the dusk edge of the main plume would have had to rotate backwards, counter to the expected dayside corotation. Due to the EUV data gap the origin of the 18 June double plume may remain unexplained.

We have already made the general observation that EUV images following extended quiet periods contain a great deal of spatial structure. The images of 18 June 2001 suggest that convection tends to smooth out or suppress spatial structure. The inverse is apparently true: in the absence of the influence of convection, the plasmasphere evolves toward a state of more complex spatial structure, as proposed by *Moldwin et al.* [1994]. On 18 June the strength of convection seemed to vary both spatially and temporally (guided, to zero-order, by the IMF polarity). We commented earlier (Section 2.2.1) that the initial 0010 UT plasmasphere (Plate 1a, Plate 2a) was more highly structured on the dayside than on the nightside, and how this seemed to be re-

lated to a weak sunward convection whose effects were only felt on the nightside. A similar effect occurred during the plume narrowing phase. Although the nightside plasmapause MLT shape was quite smooth during plume narrowing (panels e through g of Plate 1), the post-dawn plasmapause developed 0.25 R_{E} radial variations that were called 'crenulations' by *Spasojević et al.* [2003]. These crenulations first appeared near the dawn terminator and grew as they rotated eastward toward noon (see Plate 2, panel g and Plate 1, panels e through i). After an extended period of steady convection, the nightside plasmapause should be expected to coincide roughly with the location of the CCB. At this boundary, sunward convection either compresses the plasmapause or smooths its shape via azimuthally-directed flows. On the dayside, however, the plasmapause may lie inside the CCB, permitting meso-scale density structures to grow in two possible ways. First, the region inside the CCB typically exhibits a radial shear in the azimuthal/rotational flow, and this flow shear might act to distort density fluctuations that are already present. Second, the E-field inside the CCB might contain eddy-like features that encourage density structure to increase. Thus, the presence of convection at some MLTs seems to suppress the formation of sub-global density variations, while its absence at other MLTs permits these density variations to grow. Temporal relaxation of the convection field also seems to encourage the growth of complexity in the plasmaspheric density distribution. Between 1500 UT and 1830 UT, during which time the IMF remained northward, the plasmapause developed a very wavy structure, and preserved or enhanced the dayside crenulations (Plate 2k). The double plume developed a kink at about $L = 4$ and 1800 MLT; inside of $L = 4$ the plume pointed along the Y-axis, and outside $L = 4$ it bent over toward the $+X$-direction.

One possible explanation for why fine structure should be less evident in regions of strong flow, and more evident in regions of weak flow, is the following. Plasmaspheric plasma flows along $E \times B$ streamlines. Ignore, for the moment, that the plasmapause is quite structured, that in many cases a distinct 'plasmapause' cannot be identified, and that in a very structured, time-varying convection field, streamlines can cross the plasmapause boundary at angles approaching 90 degrees. In this restrictive scenario, streamlines can be oriented roughly parallel to a globally smooth plasmapause. Now imagine sub-global plasmaspheric features that modify this smooth plasmapause, such as bumps, bulges, or notches. Different parts of a given sub-

global plasmaspheric feature lie on different streamlines. When streamlines converge as the flow enters a strong flow region, the plasmaspheric features shrink in the dimension perpendicular to the streamlines. Then when the flow lines diverge as the flow velocity decreases, the features grow again in that perpendicular dimension. This could, for example, explain the formation of crenulations, which occur just past the dawnside terminator, where flow lines presumably diverge, expanding the radial extent of pre-existing MLT-variations in the plasmapause radius.

As mentioned twice earlier (Sections 1 and 2.2), the EUV instrument only sees the portion of the plasmaspheric He$^+$ ions corresponding to total (electron) number densities of 40 cm^{-3}. Plasmaspheric density generally drops with L value, so that given typical plasmaspheric distributions, the phenomena presented in this paper are primarily inside of geosynchronous orbit and hence give little if any information on the dynamics of plasma between geosynchronous orbit and the magnetopause. It is in this outer region that magnetospheric electric fields can become more highly variable both spatially and temporally due to their proximity to the auroral zone. This variability can (and undoubtedly does) introduce a complexity in the dynamic motion of the low energy plasma as it drifts toward the magnetopause. The increase of structural complexity as one moves outward in L shell is hinted at in images. For example, in Plate 2k the 'speckled' nature of the signal intensity in the plume becomes more pronounced in the vicinity of geosynchronous orbit, and just outside geosynchronous orbit and between 1500 MLT and 1700 MLT, there are some isolated green pixels that are suggestive of blob-like structure that might emerge more fully at densities below the EUV threshold, and closer to the magnetopause. These limitations of the current capabilities of plasmasphere imaging must be kept in mind when comparing modern imaging results with previous direct measurements by missions such as OGO, ISEE, and GEOS.

In the next section we examine the 18 June 2001 plasmaspheric dynamics using electric fields inferred from the plasmapause motion.

2.3. Plasmapause Electric Field

The top panel (a) of Plate 3 shows the plasmapause radial location $R_{\rm P}$ at midnight MLT, versus UT. Between 0324 UT and 0709 UT the negative $R_{\rm P}$ vs. UT slope indicates inward motion of the plasmapause during the sunward surge and plume formation stage of the 18 June erosion. Using the technique of *Goldstein*

Plate 3

et al. [2004c, b] it is possible to infer from this plasma-pause motion the electric field E_π, defined as the component of the total E-field that is tangent to the moving plasmapause. It must be noted that the direction of E_π is defined by a non-standard, time-varying coordinate system that follows the plasmapause in the counterclockwise direction. For a purely circular plasmapause, E_π is equal to E_φ, and positive (negative) E_π corresponds to outward (inward) radial motion. At the western edge of a plume, where the plasmapause can be approximately radial, E_π is approximately equal to E_r, and positive (negative) E_π corresponds to westward (eastward) azimuthal motion. For an arbitrarily shaped plasmapause, E_π includes contributions from both E_r and E_φ. Although E_π does not intrinsically contain information about the motion of plasma along the plasmapause boundary, it is possible to infer such motion from E_π by tracking the azimuthal propagation of distinct plasmapause features [*Goldstein et al.*, 2004c, b]. Because E_π provides only partial information about the electric field, care must be taken when interpreting E_π signatures, as demonstrated in the following analysis.

Plate 3b contains a keogram-style plot of E_π versus MLT and UT. The color gives E_π in mV/m, according to the scale in the legend located in the center of the plot (also see relevant text in the caption). Inward motion of the nightside plasmapause shows up in E_π as red and yellow, outward motion is given by dark blue, and a stationary plasmapause produces a cyan (i.e., light blue) E_π signature.

2.3.1. Initial (Quiet) Phase Prior to 0243 UT (in the 'Initial' phase), the mostly cyan color indicates that the nightside plasmapause between 2100 MLT and 0600 MLT was not moving, reflecting the mild, steady sunward convection prior to the erosion event (as discussed in Section 2.2.1). On the dayside, the plasmapause shape corotated, mostly undistorted except for a mild outward motion of the dayside bulge (see Plate 2a). West of the dayside bulge was a shallow notch, which also corotated. The motion of the western edge of this notch left an observable feature in E_π, the diagonal blue feature between (0010 UT, 0900 MLT) and (0200 UT, 1100 MLT). The blue color of this feature corresponds to positive E_π, which is consistent with the notch's geometry and motion. At the western edge of the notch, positive E_π is by definition composed of a negative E_r component and a positive (eastward) E_φ component. As the notch rotated eastward past a given MLT, the plasmapause at this fixed MLT would appear to move eastward (negative E_r) and outward (positive E_φ). For reference, a bold line whose slope is that of strict coro-

tation (1 MLT-hour/1 UT-hour) is drawn starting at
0600 MLT; by inspection, the slope of the blue diagonal feature is the same as the bold line. Thus, the post-
dawn plasmapause was strictly corotating while the pre-
dawn plasmapause was held stationary by steady mild
convection.

2.3.2. Sunward Surge (Erosion Onset) The onset of
the erosion first appears in Plate 3b at 0324 UT as a
burst of negative E_π (red/yellow color) centered just
east of midnight MLT. (Recall that the actual erosion
probably began 10 minutes earlier, but the image quality at 0314 UT was too poor to infer E_π). In the period
0324 UT to 0659 UT the E_π 2D plot contains several
bursts of red/yellow distributed in UT and MLT. These
bursts reflect the fact that the plasmapause inward motion did not happen smoothly and uniformly. Instead,
plasmapause motion was modulated by ϵ_{SW} (i.e., IMF
polarity), and at any given UT was localized in MLT.
Plate 3c contains a plot of ϵ_{SW}; after 0300 UT there
were three distinct intervals of negative ϵ_{SW} (i.e., southward IMF), labeled 'I', 'II' and 'III'.

Interval I began the erosion at 0314 UT, and ended
with a sharp upward turning of ϵ_{SW} at about 0400 UT
that was preceded by a gradual increase in ϵ_{SW}. The
E_π plot (Plate 3b) shows that the pre-midnight plasmapause was indented (red/yellow color) at the beginning
of interval I, but this inward motion tapered off about
30 minutes after the onset.

Interval II initiated a second burst of inward motion
at 0415 UT, also centered east of midnight MLT. The
initial indentation of this second burst then apparently
propagated both eastward (toward dawn) and westward
(toward dusk) along the plasmapause, creating the signature that looks like the letter 'V' rotated 90 degrees
clockwise. (This rotated V signature is emphasized in
Plate 3b with black and white dotted lines.) Similarly,
interval III also initiated an indentation, this time centered closer to midnight MLT, that then propagated
both eastward and westward along the plasmapause.

Between 0618 UT and 0638 UT, as the interval III
eastward-propagating indentation reached 0600 MLT
another burst of inward motion occurred near midnight,
just after another negative excursion in ϵ_{SW} (and presumably, another intensification of DMR-driven convection).

The V-shaped signatures indicate something about
the process whereby the new plasmapause formed on 18
June 2001. Each interval of negative ϵ_{SW} (which corresponds to a distinct increase in DMR convection) initiated a new indentation of the nightside plasmapause.
At the onset of erosion (0314 UT) the indentation pro-

cess tapered off 30 minutes after the convection increase. For Intervals II and III the indentation widened across the nightside; at the edges of the widening indentation were eastward-moving and westward-moving ripples that create the V-shaped signature. Careful examination of the EUV plasmapause images during the erosion verifies that the E_π analysis brings out features that are actually in the image sequence (and not an artifact), but very hard to detect by visual inspection alone.

The bursts of erosion also may shed light on the process of shielding and penetration electric field. The fact that the initial erosion (interval I) tapered off after 30 minutes is consistent with estimates for the shielding time scale [*Kelley et al.*, 1979; *Senior and Blanc*, 1984; *Goldstein et al.*, 2003d]. The burstiness of the inward motion also fits with a shielding picture. The UT-width of any of the red bursts in Plate 3b, measured at a given MLT, is between 20 and 30 minutes, even though the intervals of negative ϵ_{SW} (I, II, and III) are between 40 and 60 minutes. The propagation of the indentation may indicate the finite speed of propagation of the sunward convective impulse, or it may in fact indicate that shielding does not develop over the entire inner magnetosphere at the same time. This is not unreasonable when one considers that shielding is accomplished via coupling between the ring current and ionosphere, and the distribution of ring current ions itself varies during a convection event. The bursts are generally more intense in the midnight-to-dawn MLT sector, consistent with statistical and theoretical models that show a concentration of the penetration E-field in this sector [*Carpenter et al.*, 1972, 1993; *Carpenter and Smith*, 2000; *Senior and Blanc*, 1984; *Fejer and Scherliess*, 1995].

The ratio of E_π to ϵ_{SW} can be taken as an estimate of how much of the dawn-to-dusk solar wind E-field was transmitted to the inner magnetosphere during the erosion. We calculated the average value of E_π versus UT over the entire nightside; in Plate 3c the average $E_\pi \times 5$ has been plotted on the same axes as ϵ_{SW}. The transmission factor was apparently between 10 and 20 percent, roughly consistent with the results of *Goldstein et al.* [2004c, 2003b].

2.3.3. Late-Stage Plasmasphere Evolution   We next discuss the evolution of the plasmasphere during the latter part of the plume narrowing phase, and the plume rotation (quieting) phase. This late-stage period is slightly more complex than the sunward surge phase, with different behavior on dayside and nightside.

2.3.3.1. Nightside Plasmasphere   After 1200 UT there were two positive ϵ_{SW} excursions (i.e., northward IMF

turnings), labeled 'IV' and 'V' in Plate 3c. Following each of these positive excursions, the nightside plasmapause moved outward for about 1 UT hour, as indicated by the roughly vertical blue bands that coincide with intervals IV and V. In Section 2.2.4 it was suggested that this outward motion may have been caused by rotation of the larger duskside plasmapause into the post-midnight sector. However, such a rotation would produce a visible diagonal blue signature prior to intervals IV and V. The clear absence of such a diagonal signature before interval IV in Plate 3b means that the outward plasmapause motion was due to a positive radial flow of nightside plasma. *Carpenter et al.* [1972]; *Carpenter and Smith* [2000] observed that after temporally isolated substorms, nightside plasmaspheric plasma flowed antisunward, and speculated that this was due to the overshielding effect [*Kelley et al.*, 1979]. Overshielding occurs following a convection decrease that occurs faster than the shielding time scale; upon the lessening of convection, the residual shielding field (which has not yet had time to dissipate) imposes antisunward convection upon the inner magnetosphere. It has been demonstrated that overshielding can cause a bulging out of the midnight-to-dawn plasmapause, creating plasmaspheric shoulders [*Goldstein et al.*, 2002, 2003d]. It was apparently the case that overshielding, or some form of 'reverse' (i.e., antisunward) convection, caused the outward plasmapause motion in interval IV.

After interval IV the IMF turned southward again, producing the negative ϵ_{SW} excursion between 1330 UT and 1430 UT, and enhancing DMR convection. During this post-interval-IV convection enhancement, the nightside plasmapause ceased moving outward (E_π close to zero, cyan color), and moved slightly inward (E_π slightly negative, yellow/red color). The small amount of inward motion was localized to the pre-dawn MLT sector, again suggesting a concentration of penetration E-field. Although ϵ_{SW} during 1330–1430 UT (after interval IV) was comparable to that during intervals I and II, the effect (as reflected in E_π) of this later convection increase was much smaller. According to the DMR convection picture, after several hours of strong convection (which had occurred during 0600-1200 MLT), further strong convection has a lessened effect. This argument is strengthened by the fact that the magnitude of ϵ_{SW} during 1330–1430 UT was smaller than that of the strongest convection at earlier times.

After 1430 UT (interval V), the effects of northward IMF (positive ϵ_{SW}) dominated the nightside. The DMR convection reduction at the start of interval V caused a second outward plasmapause motion, also apparently

related to overshielding. This outward motion created a nightside plasmapause bulge that proceeded to rotate eastward at a rate commensurate with strict corotation (as indicated by the bold diagonal line in Plate 3b). This nightside corotation continued until about 1830 UT, when ϵ_{SW} again became negative. This increase in DMR convection coincided with a more pronounced inward plasmapause motion than that between intervals IV and V. About four hours of reduced convection before the 1830 UT negative ϵ_{SW} excursion increased the nightside plasmapause radius by almost 1 R_E, as discussed in Section 2.2.4, and it may have been the presence of this larger nightside plasmasphere that most likely increased the effectiveness of the post-1830 UT convection. But the diffuse yellow/red diagonal band between (1600 UT, 2100 MLT) and (2000 UT, 0100 MLT) suggests that a region of reduced plasmapause radius (i.e., a shallow notch) rotated into the post-midnight region about the same time as the convection enhancement, and thus contributed to inward plasmapause motion there.

2.3.3.2. Dayside Plasmasphere   In contrast to the nightside plasmapause behavior, which was very much driven by changes in ϵ_{SW}, the dayside plasmasphere (from 0600 MLT to 1800 MLT) corotated after 1200 UT. We infer the rotation rate from E_π by tracking the azimuthal (MLT) motion of distinctive dayside features such as the plume and crenulations, which have recognizable diagonal E_π signatures (i.e., red and blue diagonal bands at the top and bottom of Plate 3b). Judging from the slope of the diagonal signatures as compared to the slope of the line indicating strict corotation, the plasmasphere east of 0600 MLT and west of noon MLT (at the bottom part of the plot in Plate 3b) strictly corotated with the Earth. There is evidence of some slight subcorotation (shallower MLT/UT slope) west of 1800 MLT and east of noon MLT (at the top of Plate 3b). This subcorotation could be attributed to the presence of duskside convection (both DMR-driven and SAPS-driven) which is directed opposite to eastward corotational flows.

3. Simulation 18 June 2001

In this section we simulate the response of the plasmasphere to a simple global convection field driven by dayside magnetopause reconnection. Plasmaspheric dynamics can be modeled by assuming that the plasmapause boundary is composed of cold test particles subject only to $E \times B$ drift. In a time-varying electric field such as is expected in response to the variable rate of DMR, plasmapause evolution is simulated by

the changing shape of the curve defined by the aggregate of these test particles. This approach, used by *Grebowsky* [1970], *Chen and Wolf* [1972], and others, will hereinafter be called the plasmapause test particle (PTP) simulation. The PTP method is best applied to represent steep outer plasmaspheric density gradients, because a boundary with an indistinct edge (i.e., a gradually dropping density) is not well represented by a single plasmapause contour. This method is adaptive; as the PTP plasmapause curve evolves in time, test particles are added or removed as necessary to resolve its structure. Thus, the PTP simulation preserves structure without numerical diffusion; the shape of the evolving PTP plasmapause depends entirely on the initial conditions, and the details of the time-varying E-field used to drive the simulation. For initial conditions, we used a 40-term Fourier expansion of the extracted plasmapause of 0010 UT (Plate 2a).

To drive our simulation of 18 June 2001, we chose the simple and popular model of *Volland* [1973] and *Stern* [1975]. This model is not necessarily the most realistic, but if properly normalized to the solar wind electric field it is a good representation of the DMR-driven convection paradigm. The Volland-Stern (VS) model potential is $\Phi_{VS}(r, \varphi) = -A_0 \; r^2 \sin \varphi$. We normalized this function so that $A_0 = 0.2 \, |\epsilon_{SW}| \; (6.6 \, R_E)^{-1}$, which is equivalent to 20 percent of the solar wind electric field applied across the inner magnetosphere inside geosynchronous orbit. We chose 20 percent from the upper limit of the ratio E_π / ϵ_{SW} that we found from Plate 3c. To include a finite viscous interaction between the solar wind and magnetosphere during northward IMF, $|\epsilon_{SW}|$ in the VS model is constrained to be ≥ 0.5 mV/m.

Kp-based normalizations (e.g., *Maynard and Chen* [1975]) parameterize the VS model according to all the different geomagnetic phenomena that might contribute to Kp. These phenomena would include not only DMR-driven convection, but also internal magnetospheric processes like substorms and SAPS. Our ϵ_{SW}-based normalization allows us to parameterize only the DMR-driven portion of convection. The goal of our simulation is to present the response of the plasmasphere to a simplified global DMR-driven convection E-field. We will compare this DMR-driven response to the real response of the plasmasphere as seen by EUV, in order to study the limits of the validity of the DMR convection picture.

The results of the 18 June 2001 PTP simulation are presented in Plate 4 and Plate 5, which are formatted similarly to Plate 1 and Plate 2, respectively. The panel labels (a through l) and time stamps are the same for

Plate 4

Plate 5

the EUV and PTP figures. Comparison of the EUV images and PTP simulated plasmapause curves reveals both similarites and differences.

The most obvious agreement is the global behavior of the plasmasphere during active times. The PTP simulated plasmasphere evolves according to the same phases of plume formation and evolution as the EUV imaged plasmasphere. The erosion begins when ϵ_{SW} turns negative (i.e., the IMF turns southward) and DMR-driven convection becomes strong. Sunward surging on both nightside and dayside produces a reduced nightside plasmapause radius, and a broad dayside plume. Over the course of several hours, the initial surge plume then narrows in local time, and the edges of the plume (both dusk and western) are in reasonable agreement with the EUV data, although the PTP model dusk edge is at a slightly larger Y value than that of EUV. With reference to the discussion of the 3–4-mV/m ϵ_{SW} oscillations in Plate 3, note that between 1215 UT (Plate 5e) and 1316 UT (Plate 5f) the dusk edge of the plume (at the dusk terminator, 1800 MLT) moves outward in Y by about 0.4 R_E in response to the positive ϵ_{SW} excursion between these two times. Plume rotation and wrapping commences after 1500 UT in the model, although during this quieting phase the PTP-EUV differences become more severe (as we will discuss below).

In the PTP model, some of the structure (especially in the early sunward surge phase) depends on the initial conditions; e.g., the duskside bulge at 0010 UT (Plate 4a) evolves into a spiky structure near dusk at 0436 UT (Plate 4b). This is consistent with the long-standing idea that at a given instant of time, the plasmaspheric configuration reflects the time-integrated effects of a few or several previous hours of geomagnetic conditions. Thus, plasmapause models often depended not on instantaneous Kp, but rather some representation (e.g., maximum or average) of a few or several previous hours of Kp (e.g., *Carpenter and Anderson* [1992]). However, in the PTP simulation most of the original spatial structure is eventually washed away during the erosion, and the final state of the plasmasphere is dominated by the spatial form of the VS electric field model, normalized to the time-varying solar wind E-field. Said another way, the global properties of the plasmasphere (which is all one can hope to capture when using the VS model which does not contain any sub-global spatial variation of the inner magnetospheric E-field) are indeed directly driven by the state of dayside magnetopause reconnection-driven convection. The sub-global scale features of the plasmasphere must then depend on the prior history of the plasmasphere and/or the sub-global

spatial structure of the convection field.

It is on the sub-global scale that the PTP simulation differs from the EUV plasmasphere evolution of 18 June 2001. The absence of SAPS in the Volland-Stern potential means that the location of the duskside edge of the PTP plume is eastward of the EUV-observed location. Also, the narrow duskside plume of Plate 2c fails to develop in the PTP simulation, again presumably due to the lack of SAPS to strengthen sunward convection near dusk. Instead of the narrow duskside plume, the PTP simulated plasmapause of Plate 5c has a spiky bulge (mentioned in the previous paragraph) near 2100 MLT that is a remnant of the large duskside bulge of Plate 5a. This spiky feature then gets compressed by nightside convection and rotates across the nightside, reaching 0300 MLT by 1418 UT (Plate 5g). In the EUV images there is no such rotating spiky feature because in the EUV plasmasphere the initial duskside bulge is elongated by strong duskside (SAPS) convection into a narrow duskside plume (see Plate 2c and *Goldstein et al.* [2003b]).

The compression of this spiky feature is interesting because it shows that under the right circumstances, sub-global spatial structure (in the plasmaspheric density distribution) can survive the trip across the nightside even during strong sunward convection. If such a structure were in fact present on the nightside plasmapause in EUV images, it would not be resolved by the 0.1-R_E EUV pixels. When convection is relaxed, this structure would be free to expand again inside the corotation/convection boundary (CCB). This could be a partial explanation for why the plasmasphere seems to develop increased spatial structure as soon as convection drops off; the structure is compressed by the contraction of the CCB that accompanies strong convection, but it survives and gets elongated or distorted once free to evolve inside an expanded CCB. In this scenario, plasmapause crenulations form in the post-dawn MLT sector where the plasmapause lies inside the CCB, and wavy variations of the plasmapause develop during the quieting (plume rotation/wrapping) phase. (This hypothetical scenario was mentioned earlier, at the end of the section titled 'Sub-Global Plasma Structures.')

This brings up the next point: if the PTP simulation preserves structure, and if that structure can survive strong convection intervals, why doesn't the double plume develop in the PTP model, and why is the PTP model so much less structured during the plume rotation phase? One explanation might be that the initial conditions failed to capture all of the (perhaps sub-EUV-pixel) structure of the 0010 UT plasmasphere, and

some of this uncaptured structure becomes important in later stages of the evolution. Even if this is the case (and it quite probably is), it is also undeniably true that the Volland-Stern model is too simple to properly capture anything but global plasmasphere evolution, and so it is not surprising that the double plume, the crenulations, and other meso-scale and fine-scale features are not reproduced. Besides SAPS, another important known effect not included in the VS model is the concentration of electric field in the midnight-to-dawn MLT sector. This effect is quite evident in the E_π 2D plot of Plate 3b. To highlight this difference more quantitatively, Plate 6 shows R_P versus MLT plots of both EUV and PTP plasmapauses taken from the four panels (a, c, g, and k) of Plate 2 and and Plate 5. By visual inspection it is clear that during the sunward surge phase (Plate 6c), the inward plasmapause motion between midnight MLT and 0600 MLT is more pronounced for the EUV plasmapause (blue circles) than the PTP model plasmapause (bold line). It is midnight-to-dawn convection concentration that apparently produces the flattening and indentation evident in panels b, c, and d of Plate 1, and in Plate 2b. This flattening is not apparent in the PTP model snapshots of Plate 4, panel b, c, and d, Similarly, the outward bulging evident in the EUV midnight-to-dawn plasmapauses of Plate 6g and Plate 6k is absent in the PTP model plasmapauses of the same MLT range. This demonstrates the necessity for a more sophisticated (i.e., MLT-dependent) treatment of the penetration E-field than that of the Volland-Stern model.

Plate 6

The observed quiet-time meso-scale and fine-scale complexity of the plasmaspheric density distribution deserves much more attention. The EUV images suggest a level of fine-scale structure that is unresolved by the 0.1 R_E EUV pixels, and this is in agreement with the very structured density profiles that have been observed in situ [*Moldwin et al.*, 1994, 1995; *Carpenter and Lemaire*, 1997]. Plasma instabilities and other subtle (non $E \times B$-driven) physics may very well be involved in the quiet-time plasmasphere evolution, when DMR-driven convection is mild or completely absent.

4. CONCLUDING REMARKS

4.1. Alternate Plume Formation Mechanism

We have shown that the global pattern of plume evolution observed on 18 June 2001 fits with the DMR-driven convection picture. An alternate plume formation scenario was proposed by *Lemaire* [2000], in which a plasmapause bulge forms on the dayside and subsequently evolves into a duskside plume. Because rotation

speed decreases with radial distance, the bulge experiences a shear in the eastward convection speed, and it gets stretched/distorted into a plume. This scenario was apparently verified by EUV observations on 10 June 2001 [*Spasojević et al.*, 2003].

4.2. Comments on Interchange Driven Erosion

The validity of the DMR-driven convection picture relies on the assumption that plasmaspheric plasma is subject only to $E \times B$-drift in a global convection field, and lacking complete knowledge of the inner magnetospheric E-field, it is not known precisely how the new plasmapause boundary forms, especially during an erosion. As mentioned in Section 1, *Lemaire* [1975] proposed that the plasmapause forms under the influence of small-scale electric fields that arise due to the gravitational/centrifugal interchange instability. One of the predictions of this hypothesis is that during an erosion, the nightside plasma at the boundary moves radially outward, detaching from the main plasmasphere as blobs. The gradual removal of a large number of blobs produces a net inward motion of the plasmapause [*Lemaire and Gringauz*, 1998]. The maximum allowable speed of the interchange-driven blob was estimated by *Lemaire and Gringauz* [1998] to be about $V_{\max}$=0.03 R_{E}/hour.

To date, EUV images acquired during erosion have revealed no evidence of this proposed outward motion of detached parcels of nightside plasma. In fact, all of the evidence in EUV images suggests that plasma motion is sunward; both the dayside and nightside boundaries move sunward during the initial stage of the erosion. Because EUV cannot see low-density plasma below 40 cm^{-3}, it is conceivable that the nightside blobs are invisible to the EUV cameras because as they move radially outward, their density quickly drops below the lower density threshold. Let us examine this premise in the context of the 18 June 2001 event. In Plate 3a is a plot of R_{P} versus UT, showing the initial plasmapause location at $L = 4.4$ at 0325 UT. Suppose that the plasmapause plasma moves outward, and as it does, its density drops according to the inverse of the flux tube volume, i.e., L^{-4}. If we assume the plasmaspheric density of *Carpenter and Anderson* [1992], this outermost plasma parcel has electron density of about 295 cm^{-3}. In order for the plasma parcel to become invisible to EUV, its final density must be $\leq$40 cm^{-3}. Then its final L-shell is $L_f \geq L_i \, (295/40)^{-\frac{1}{4}}$, or $L_f \geq 7.2$. For this outward motion to avoid being captured by EUV, it must travel to this final location L_f in 10 minutes or less (the time cadence of EUV images); the plasma par-

cel must have speed $V_f \geq 2.8\,R_{\mathrm{E}}/10$ min., or $17\,R_{\mathrm{E}}/$hr. The lower limit of the required speed is 570 times faster than $V_{\max}$, the maximum interchange speed. Even if the proposed blobs are of a size that is below the resolution of the EUV imager, to account for the large amount of nightside cold plasma that is removed during erosion, a large number of blobs would be required. One would still expect to see the collective motion of such a large number of tiny blobs with a poorly-resolved image, just as a person with poor vision can still see the collective motion of a large number of individual drops of rain, or individual grains of sand on a windy day.

Thus, the invisible outward-moving blob scenario seems unlikely, for the following reasons. First, the dayside plasmasphere expands/rarefies during erosion, and still remains visible to EUV at geosynchronous orbit and beyond [*Goldstein et al.*, 2004b]. Second, it is not probable that the blobs could move fast enough to avoid leaving some detectable signature in EUV images. Other than a pixelated noise background with no evidence of systematically outward-moving blobs, the nightside in EUV images typically appears to be evacuated of plasmaspheric plasma exterior to the inward-moving plasmapause during erosions (e.g., see Plate 1). Third, if one supposes that the blobs have density below the EUV threshold when they first detach from the surrounding dense nightside plasmapause, or that they are of a spatial size too small to be resolved by EUV (and thus they are invisible to EUV at all times), then it is difficult to account for the large amount of dense nightside plasmaspheric plasma removed during the erosion by such tenuous blobs. With its slow growth rate, the interchange instability probably does not play a strong role during geomagnetically active times. On the other hand, the role of interchange during extended quiet periods ought to be investigated further, because during such periods slower processes may have enough time to act effectively.

Summary

The 18 June 2001 EUV observed erosion event serves as an example of the global-scale pattern of plume evolution that is repeatedly found in plasmasphere images during geomagnetically active times. Given an initial plasmaspheric configuration that is subject to an increase in the strength of sunward convection, plume formation and evolution follows three main phases: sunward surge, plume narrowing, and plume rotating/wrapping. The excellent EUV image coverage of the 18 June event contains examples of all of these phases from a single erosion event. On a global scale, the 18 June plasmas-

phere observations are consistent with the DMR-driven convection interpretation, as represented by both prior modeling work by *Grebowsky* [1970] and others, and by our own simulation specifically tailored for the 18 June event. The EUV observations of this event are also consistent with prior in situ observations of shrinking plasmaspheres, detached plasma regions, and duskside bulge rotation [*Moldwin et al.*, 2003].

On a sub-global scale, proper treatment of plasmaspheric dynamics requires a more sophisticated treatment than offered by the global DMR-driven convection picture. A handful of interesting sub-global plasmaspheric features were observed on 18 June; some of these features have plausible explanations. The narrow duskside plume (Plate 2c) and sharpening of the duskside plasmapause (e.g., Plate 1d) both indicate the presence of SAPS, a coupling phenomenon not directly driven by dayside reconnection. The pre-dawn indentation (e.g., Plate 1d) or flattening (Plate 2c) suggests the presence of pre-dawn concentration of the penetration electric field [*Carpenter and Smith*, 2000]. Similarly, the outward excursion of the midnight-to-dawn plasmapause during northward IMF (i.e., positive ϵ_{SW}) probably reflects the presence of overshielding [*Carpenter and Smith*, 2000].

Other features defy immediate explanation. The plume bifurcation (or double plume) and crenulations (both in Plate 2g) might arise due to spatial structure in the initial (pre-erosion) plasmasphere, or might be created by spatial structure in the dayside convection field. The increased spatial structure and complexity in the plasmaspheric distribution during the quieting phase (plume rotating/wrapping) is similarly unexplained. Does this spatial structure arise due to density fluctuations in the initial plasmasphere that grow and change shape? Is the structure due to spatially structured quiet-time electric fields? Or is it due to plasma instabilities and non-$E \times B$ motion? Whatever the cause of meso-scale and fine-scale density variations in the plasmasphere, general EUV observations, and the 18 June images in particular, suggest that convection suppresses or smooths the structure, while the absence or lessening of strong convection seems to encourage its growth.

Our electric field (E_π) analysis yielded some insight into the process of erosion. The rotated-V signatures (Plate 3b) suggest that during the early phase of the erosion, there is partial indentation of the plasmapause near or east of midnight MLT, with subsequent eastward and westward spreading/widening of the indentation, as discussed by *Carpenter and Lemaire* [1997] and

similarly observed by *Goldstein et al.* [2004c, a]. We observed bursts of erosion whose intensity was modulated by the sign of ϵ_{SW} (a time-delayed proxy for the IMF polarity). Some of the bursty behavior suggests a shielding time scale of 20–30 minutes, and the midnight-to-dawn concentration of the bursts probably reflects pre-dawn concentration of the penetration E-field. From our E_π analysis we estimated two quantities. The time delay $\Delta\tau_C$ between IMF polarity reversal at the magnetopause and the resulting motion of the plasmapause was found to be 10 ± 20 minutes. The inner magnetospheric E-field was found to be about 10–20 percent of the solar wind E-field. During the later phase of the erosion (once the sunward surge was over), we observed different behavior on the dayside and nightside. The dayside tended to corotate, independent of ϵ_{SW} polarity. The nightside behavior was modulated by ϵ_{SW}. When $\epsilon_{SW} < 0$, mild sunward motion occurred, less pronounced than in the early stages of the erosion. When $\epsilon_{SW} > 0$, apparent overshielding caused an outward bulging of the midnight-to-dawn plasmapause, and this bulge subsequently corotated during extended positive ϵ_{SW}. From this event it is clear that more information about the detailed structure of the inner magnetospheric E-field is needed. There is hope that future comparisons between models and global EUV images, and EUV E_π analysis of other events, will yield insight into this electric field and its effect on the plasmasphere.

REFERENCES

Anderson, P. C., D. L. Carpenter, K. Tsuruda, T. Mukai, and F. J. Rich (2001), Multisatellite observations of rapid subauroral ion drifts (SAID), *J. Geophys. Res.*, *106*, 29,585.

Burch, J. L. (2000), IMAGE mission overview, *Space Sci. Rev.*, *91*, 1.

Burch, J. L., D. G. Mitchell, B. R. Sandel, P. C. Brandt, and M. Wüest (2001), Global dynamics of the plasmasphere and ring current during magnetic storms, *Geophys. Res. Lett.*, *28*, 1159.

Burke, W. J., A. G. Rubin, N. C. Maynard, L. C. Gentile, P. J. Sultan, F. J. Rich, O. de La Beujardière,

C. Y. Huang, and G. R. Wilson (2000), Ionospheric disturbances observed by DMSP at middle to low latitudes during the magnetic storm of June 4–6, 1991, *J. Geophys. Res.*, *105*, 18,391.

Burke, W. J., et al. (1998), Electrodynamics of the inner magnetosphere observed in the dusk sector by CRRES and DMSP during the magnetic storm of June 4–6, 1991, *J. Geophys. Res.*, *103*, 29,399.

Carpenter, D. L. (1995), Earth's plasmasphere awaits rediscovery, *EOS Trans. AGU*, *76*, 89.

Carpenter, D. L., and R. R. Anderson (1992), An ISEE/Whistler model of equatorial electron density in the magnetosphere, *J. Geophys. Res.*, *97*, 1097.

Carpenter, D. L., and J. Lemaire (1997), Erosion and recovery of the plasmasphere in the plasmapause region, *Space Sci. Rev.*, *80*, 153.

Carpenter, D. L., and A. J. Smith (2000), The study of bulk plasma motions and associated electric fields in the plasmasphere by means of whistler-mode signals, *J. Atmos. Solar-Terr. Phys.*, p. 1.

Carpenter, D. L., K. Stone, J. C. Siren, and T. L. Crystal (1972), Magnetospheric electric fields deduced from drifting whistler paths, *J. Geophys. Res.*, *77*, 2819.

Carpenter, D. L., B. L. Giles, C. R. Chappell, P. M. E. Decreau, R. R. Anderson, A. M. Persoon, A. J. Smith, Y. Corcuff, and P. Canu (1993), Plasmasphere dynamics in the dusk-side bulge region: a new look at an old topic, *J. Geophys. Res.*, *98*, 19,243.

Chappell, C. R. (1974), Detached plasma regions in the magnetosphere, *J. Geophys. Res.*, *79*, 1861.

Chappell, C. R., K. K. Harris, and G. W. Sharp (1970a), A study of the influence of magnetic activity on the location of the plasmapause as measured by OGO5, *J. Geophys. Res.*, *75*, 50.

Chappell, C. R., K. K. Harris, and G. W. Sharp (1970b), The morphology of the bulge region of the plasmasphere, *J. Geophys. Res.*, *75*, 3848.

Chen, A. J., and R. A. Wolf (1972), Effects on the plasmasphere of a time-varying convection electric field, *Planet. Space Sci.*, *20*, 483.

Coroniti, F. V., and C. F. Kennel (1973), Can the ionosphere regulate magnetospheric convection?, *J. Geophys. Res.*, *78*, 2837.

Dent, Z. C., I. R. Mann, F. W. Menk, J. Goldstein, C. R. Wilford, M. A. Clilverd, and L. G. Ozeke (2003), A coordinated ground-based and IMAGE satellite study of quiet-time plasmaspheric density profiles, *Geophys. Res. Lett.*, *30*(12), 1600, doi:10.1029/2003GL016,946.

Dungey, J. W. (1961), Interplanetary magnetic field and the auroral zones, *Phys. Rev. Lett.*, *6*, 47.

Elphic, R. C., L. A. Weiss, M. F. Thomsen, D. J. McComas, and M. B. Moldwin (1996), Evolution of plasmaspheric ions at geosynchronous orbit during times of high geomagnetic activity, *Geophys. Res. Lett.*, *23*, 2189.

Fejer, B. G., and L. Scherliess (1995), Time dependent response of equatorial ionospheric electric fields in magnetospheric disturbances, *Geophys. Res. Lett.*, *22*, 851.

Fejer, B. G., R. W. Spiro, R. A. Wolf, and J. C. Foster (1990), Latitudinal variation of perturbation electric fields during magnetically disturbed periods: 1986 SUNDIAL observations and model results, *Ann. Geophys.*, *8*, 441.

Foster, J. C., and W. J. Burke (2002), SAPS: A new catego-

rization for sub-auroral electric fields, *EOS Trans. AGU*, *83*, 393.

Foster, J. C., and H. B. Vo (2002), Average characteristics and activity dependence of the subauroral polarization stream, *J. Geophys. Res.*, *107*(A12), 1475, doi: 10.1029/2002JA009409.

Foster, J. C., P. J. Erickson, A. J. Coster, and J. Goldstein (2002), Ionospheric signatures of plasmaspheric tails, *Geophys. Res. Lett.*, *29*(13), 1623, doi: 10.1029/2002GL015067.

Goldstein, J., R. W. Spiro, P. H. Reiff, R. A. Wolf, B. R. Sandel, J. W. Freeman, and R. L. Lambour (2002), IMF-driven overshielding electric field and the origin of the plasmaspheric shoulder of May 24, 2000, *Geophys. Res. Lett.*, *29*(16), doi:10.1029/2001GL014534.

Goldstein, J., B. R. Sandel, W. T. Forrester, and P. H. Reiff (2003a), IMF-driven plasmasphere erosion of 10 July 2000, *Geophys. Res. Lett.*, *30*(3), doi: 10.1029/2002GL016478.

Goldstein, J., B. R. Sandel, P. H. Reiff, and M. R. Hairston (2003b), Control of plasmaspheric dynamics by both convection and sub-auroral polarization stream, *Geophys. Res. Lett.*, *30*(24), 2243, doi:10.1029/2003GL018390.

Goldstein, J., M. Spasojević, P. H. Reiff, B. R. Sandel, W. T. Forrester, D. L. Gallagher, and B. W. Reinisch (2003c), Identifying the plasmapause in IMAGE EUV data using IMAGE RPI in situ steep density gradients, *J. Geophys. Res.*, *108*(A4), 1147, doi:10.1029/2002JA009475.

Goldstein, J., R. W. Spiro, B. R. Sandel, R. A. Wolf, S.-Y. Su, and P. H. Reiff (2003d), Overshielding event of 28-29 July 2000, *Geophys. Res. Lett.*, *30*(8), 1421, doi: 10.1029/2002GL016644.

Goldstein, J., B. R. Sandel, M. R. Hairston, and S. B. Mende (2004a), Plasmapause undulation of 17 April 2002, *Geophys. Res. Lett.*, *31*, L15,801, doi:10.1029/2004GL019959.

Goldstein, J., B. R. Sandel, M. F. Thomsen, M. Spasojević, and P. H. Reiff (2004b), Simultaneous remote-sensing and in situ observations of plasmaspheric drainage plumes, *J. Geophys. Res.*, *109*, A03,202, doi:10.1029/2003JA010,281.

Goldstein, J., R. A. Wolf, B. R. Sandel, and P. H. Reiff (2004c), Electric fields deduced from plasmapause motion in IMAGE EUV images, *Geophys. Res. Lett.*, *31*(1), L01,801, doi:10.1029/2003GL018797.

Grebowsky, J. M. (1970), Model study of plasmapause motion, *J. Geophys. Res.*, *75*, 4329.

Higel, B., and L. Wu (1984), electron density and plasmapause characteristics at 6.6 RE: A statistical study of the GEOS 2 relaxation sounder data, *J. Geophys. Res.*, *89*, 1583.

Huang, T. S., R. A. Wolf, and T. W. Hill (1990), Interchange instability of the Earth's plasmapause, *J. Geophys. Res.*, *95*, 17,187.

Jaggi, R. K., and R. A. Wolf (1973), Self-consistent calculation of the motion of a sheet of ions in the magnetosphere, *J. Geophys. Res.*, *78*, 2852.

Kelley, M. C., B. G. Fejer, and C. A. Gonzales (1979), An explanation for anomalous ionospheric electric fields associated with a northward turning of the interplanetary magnetic field, *Geophys. Res. Lett.*, *6*, 301.

Lambour, R. L., L. A. Weiss, R. C. Elphic, and M. F. Thomsen (1997), Global modeling of the plasmasphere following storm sudden commencements, *J. Geophys. Res.*, *102*,

24,351.

LeDocq, M. J., D. A. Gurnett, and R. R. Anderson (1994), Electron number density fluctuations near the plasmapause observed by the CRRES spacecraft, *J. Geophys. Res.*, *99*, 23,661.

Lemaire, J. (1975), The mechanisms of formation of the plasmapause, *Ann. Geophys.*, *31*, 175.

Lemaire, J. (2000), The formation of plasmaspheric tails, *Phys. Chem. Earth (C)*, *25*, 9.

Lemaire, J. F., and K. I. Gringauz (1998), *The Earth's Plasmasphere*, Cambridge University Press, Cambridge.

Maynard, N. C., and A. J. Chen (1975), Isolated cold plasma regions: Observations and their relation to possible production mechanisms, *J. Geophys. Res.*, *80*, 1009.

McComas, D. J., S. J. Bame, P. Barker, W. C. Feldman, J. L. Phillips, P. Riley, and J. W. Griffee (1998), Solar wind electron proton alpha monitor (SWEPAM) for the Advanced Composition Explorer, *Space Sci. Rev.*, *86*, 563.

Moldwin, M. B., M. F. Thomsen, S. J. Bame, D. J. McComas, and K. R. Moore (1994), An examination of the structure and dynamics of the outer plasmasphere using multiple geosynchronous satellites, *J. Geophys. Res.*, *99*, 11,475.

Moldwin, M. B., M. F. Thomsen, S. J. Bame, D. McComas, and G. D. Reeves (1995), The fine-scale structure of the outer plasmasphere, *J. Geophys. Res.*, *100*, 8021.

Moldwin, M. B., B. R. Sandel, M. Thomsen, and R. Elphic (2003), Quantifying global plasmaspheric images with in situ observations, *Space Sci. Rev.*, *109*, 47.

Richmond, A. D. (1973), Self-induced motions of thermal plasma in the magnetosphere and stability of the plasmapause, *Rad. Sci.*, *8*, 1019.

Sandel, B. R., R. A. King, W. T. Forrester, D. L. Gallagher, A. L. Broadfoot, and C. C. Curtis (2001), Initial results from the IMAGE extreme ultraviolet imager, *Geophys. Res. Lett.*, *28*, 1439.

Sandel, B. R., J. Goldstein, D. L. Gallagher, and M. Spasojević (2003), Extreme ultraviolet imager observations of the structure and dynamics of the plasmasphere, *Space Sci. Rev.*, *109*, 25.

Sandel, B. R., et al. (2000), The extreme ultraviolet imager investigation for the IMAGE mission, *Space Sci. Rev.*, *91*, 197.

Scherliess, L., and B. G. Fejer (1997), Storm time dependence of equatorial disturbance dynamo zonal electric fields, *J. Geophys. Res.*, *102*, 24,037.

Senior, C., and M. Blanc (1984), On the control of magnetospheric convection by the spatial distribution of ionospheric conductivities, *J. Geophys. Res.*, *89*, 261.

Smith, C. W., M. H. Acuna, L. F. Burlaga, J. L'Heureux, N. F. Ness, and J. Sheifele (1998), The ACE magnetic field experiment, *Space Sci. Rev.*, *86*, 613.

Spasojević, M., J. Goldstein, D. L. Carpenter, U. S. Inan, B. R. Sandel, M. B. Moldwin, and B. W. Reinisch (2003), Global response of the plasmasphere to a geomagnetic disturbance, *J. Geophys. Res.*, *108*(A9), 1340, doi:10.1029/2003JA009987.

Spiro, R. W., M. Harel, R. A. Wolf, and P. H. Reiff (1981), Quantitative simulation of a magnetospheric substorm 3. Plasmaspheric electric fields and evolution of the plasmapause, *J. Geophys. Res.*, *86*, 2261.

Stern, D. P. (1975), The motion of a proton in the equatorial

magnetosphere, *J. Geophys. Res.*, *80*, 595.

Stone, E. C., A. M. Frandsen, R. A. Mewaldt, E. R. Christian, D. Margolies, J. F. Ormes, and F. Snow (1998), The Advanced Composition Explorer, *Space Sci. Rev.*, *86*, 1.

Volland, H. (1973), Semiempirical model of large-scale magnetospheric electric fields, *J. Geophys. Res.*, *78*, 171.

Weiss, L. A., R. L. Lambour, R. C. Elphic, and M. F. Thomsen (1997), Study of plasmaspheric evolution using geosynchronous observations and global modeling, *Geophys. Res. Lett.*, *24*, 599.

Wygant, J. R., D. E. Rowland, H. J. Singer, M. Temerin, F. Mozer, and M. K. Hudson (1998), Experimental evidence on the role of the large spatial scale electric field in creating the ring current, *J. Geophys. Res.*, *103*, 29,527.

J. Goldstein, Space Sci Div, Southwest Research Institute, San Antonio, TX 78228 USA (jgoldstein@swri.edu)

B. R. Sandel, Lunar and Planetary Lab, University of Arizona, Tucson, AZ 85721 USA

Figure 1.

Figure 2.

Figure 3.

Figure 4.

Figure 5.

Figure 6.

Figure 7.

PLUME EVOLUTION

GOLDSTEIN AND SANDEL

PLUME EVOLUTION

GOLDSTEIN AND SANDEL

PLUME EVOLUTION

GOLDSTEIN AND SANDEL

PLUME EVOLUTION

GOLDSTEIN AND SANDEL

PLUME EVOLUTION

GOLDSTEIN AND SANDEL

PLUME EVOLUTION

GOLDSTEIN AND SANDEL

PLUME EVOLUTION

GOLDSTEIN AND SANDEL

PLUME EVOLUTION

GOLDSTEIN AND SANDEL

PLUME EVOLUTION

GOLDSTEIN AND SANDEL

PLUME EVOLUTION

GOLDSTEIN AND SANDEL

PLUME EVOLUTION

GOLDSTEIN AND SANDEL

PLUME EVOLUTION

GOLDSTEIN AND SANDEL

PLUME EVOLUTION

GOLDSTEIN AND SANDEL

PLUME EVOLUTION

GOLDSTEIN AND SANDEL

PLUME EVOLUTION

GOLDSTEIN AND SANDEL

PLUME EVOLUTION

GOLDSTEIN AND SANDEL

PLUME EVOLUTION

GOLDSTEIN AND SANDEL

PLUME EVOLUTION

GOLDSTEIN AND SANDEL

PLUME EVOLUTION

GOLDSTEIN AND SANDEL

PLUME EVOLUTION

GOLDSTEIN AND SANDEL

PLUME EVOLUTION

GOLDSTEIN AND SANDEL

PLUME EVOLUTION

GOLDSTEIN AND SANDEL

PLUME EVOLUTION

GOLDSTEIN AND SANDEL

PLUME EVOLUTION

GOLDSTEIN AND SANDEL

PLUME EVOLUTION

GOLDSTEIN AND SANDEL

PLUME EVOLUTION

GOLDSTEIN AND SANDEL

PLUME EVOLUTION

GOLDSTEIN AND SANDEL

PLUME EVOLUTION

GOLDSTEIN AND SANDEL

PLUME EVOLUTION

GOLDSTEIN AND SANDEL

PLUME EVOLUTION

GOLDSTEIN AND SANDEL

PLUME EVOLUTION

GOLDSTEIN AND SANDEL

PLUME EVOLUTION

GOLDSTEIN AND SANDEL

PLUME EVOLUTION

GOLDSTEIN AND SANDEL

PLUME EVOLUTION

GOLDSTEIN AND SANDEL
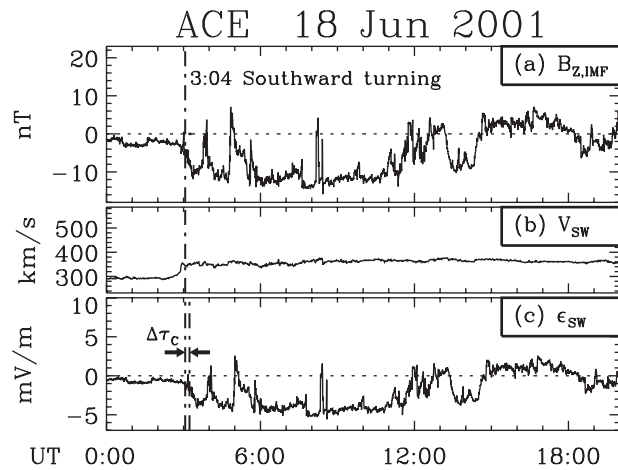
Figure 1. ACE MAG and SWEPAM data (courtesy N. Ness, C. Smith, D. McComas, and the ACE science center) on 18 June 2001, time-delayed to account for propagation to the magnetopause. (a) Z-component of the IMF $B_{Z,\mathrm{IMF}}$; (b) solar wind speed V_{SW}; (c) solar wind electric field ϵ_{SW}, delayed by $\Delta\tau_{\mathrm{C}}$ (described in text). Solar wind and IMF conditions changed at about 0300 UT, with a 0257 UT step-increase in V_{SW} and a 0304 UT southward excursion in $B_{Z,\mathrm{IMF}}$. After 0314 UT ϵ_{SW} was negative, indicating a dawn-to-dusk global electric field.
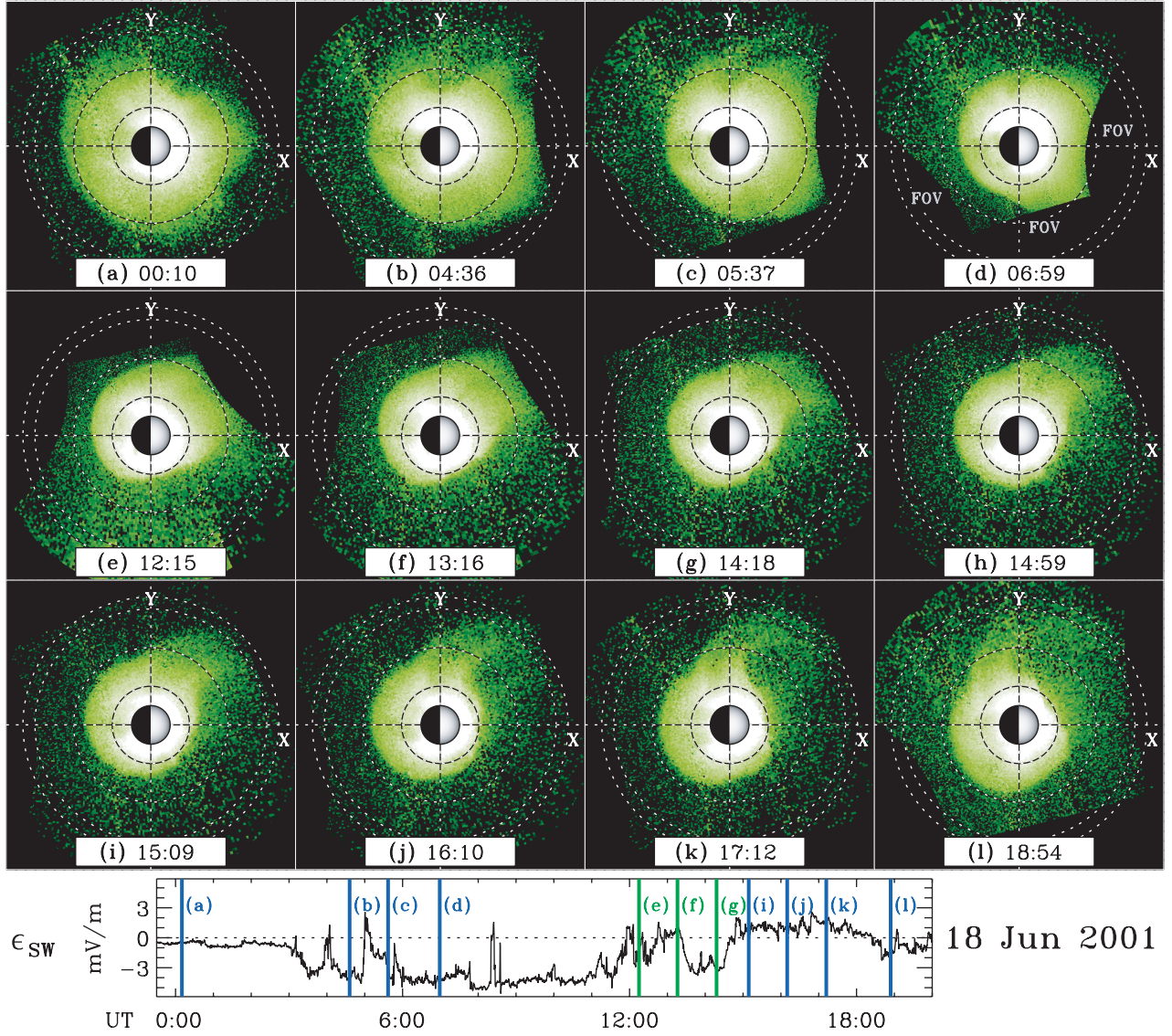
Plate 1. Panels a through l: IMAGE EUV global plasmasphere observations on 18 June 2001, depicting erosion of the plasmasphere and formation/evolution of a drainage plume. Each panel shows the equatorial plasmaspheric He$^+$ distribution versus X and Y (in SM coordinates). Color indicates column abundance (in arbitrary units), with black = zero. The Sun is to the right (positive X); the Earth is at the center. Circles are drawn at $L = 2, 4, 6$, and 6.62 (geosynchronous orbit). Bottom panel: ACE ϵ_{SW} from Figure 1c. Vertical lines labeled a through l indicate times of EUV snapshots above.

Initial   Sunward Surge   Plume Narrowing   Plume Rotating
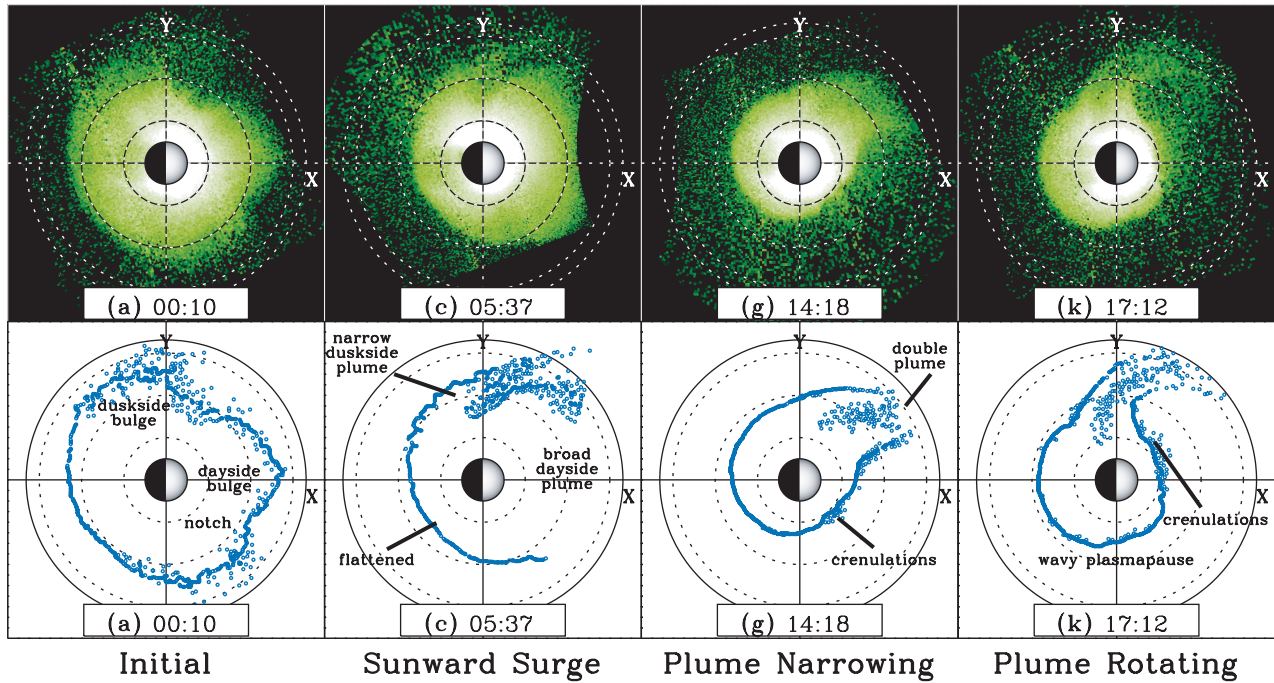
Plate 2. Top row: Four selected panels a, c, g, and k from Plate 1, each showing an EUV plasmasphere global image, as described in the caption for Plate 1. Bottom row: In each panel, the blue circles are manually extracted points from the EUV image above it, highlighting the features discussed in the text. (The apparently solid blue lines on the night side are actually composed of a very large number of blue circles.) At the bottom of each panel is a label indicating the phase of plume formation/evolution, as discussed in the text.

Plasmapause Electric Field E_π 18 Jun 2001
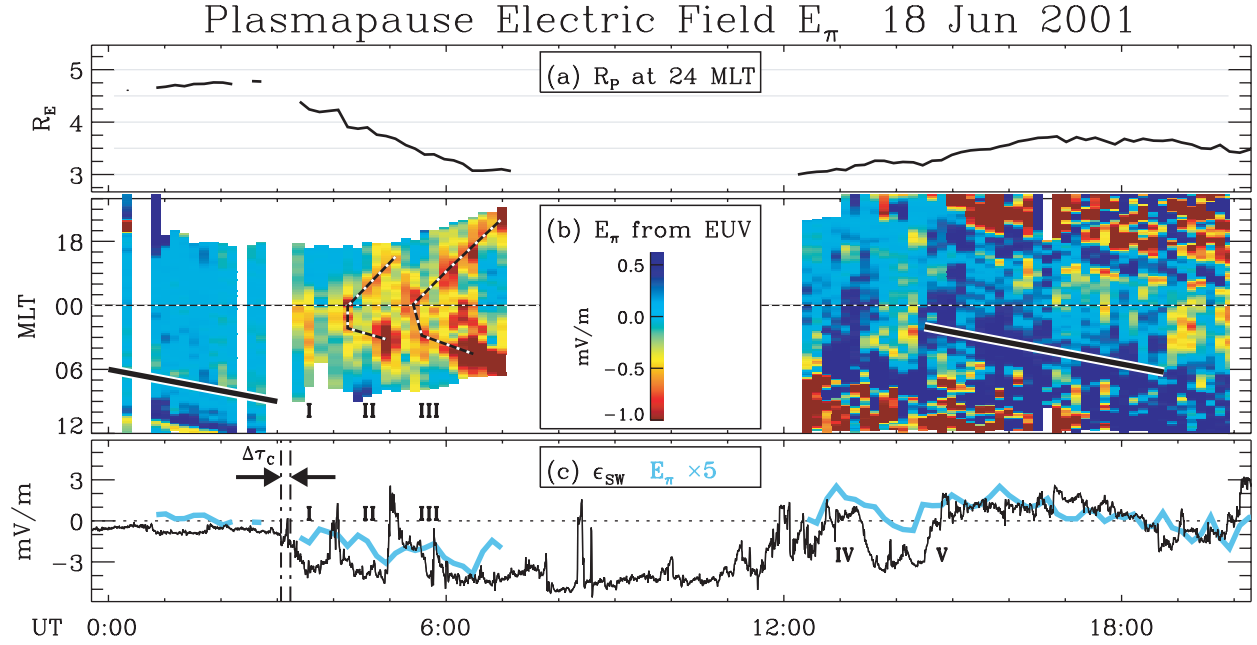
Plate 3. Electric field deduced from the motion of the plasmapause in IM-AGE EUV images, 18 June 2001. (a) Plasmapause radius versus UT, at midnight MLT. (b) E-field component E_π tangential to the moving plasmapause, versus MLT and UT. Color indicates E_π strength in mV/m: red is $E_\pi < 0$ (inward motion), blue is $E_\pi > 0$ (outward motion), cyan is $E_\pi \approx 0$ (stationary plasmapause), and white is no data. Dotted line indicates midnight (2400) MLT. Diagonal lines (before 0300 UT, and between 1430 UT and 1830 UT) indicate strict corotation (1 MLT-hour per UT-hour). (c) Solar wind E-field ϵ_{SW} from Figure 1c (black) and $E_\pi \times 5$ (blue). Ratio of ϵ_{SW} to E_π indicates approximately 10 to 20 percent of dawn-to-dusk solar wind E-field transmitted to inner magnetosphere.
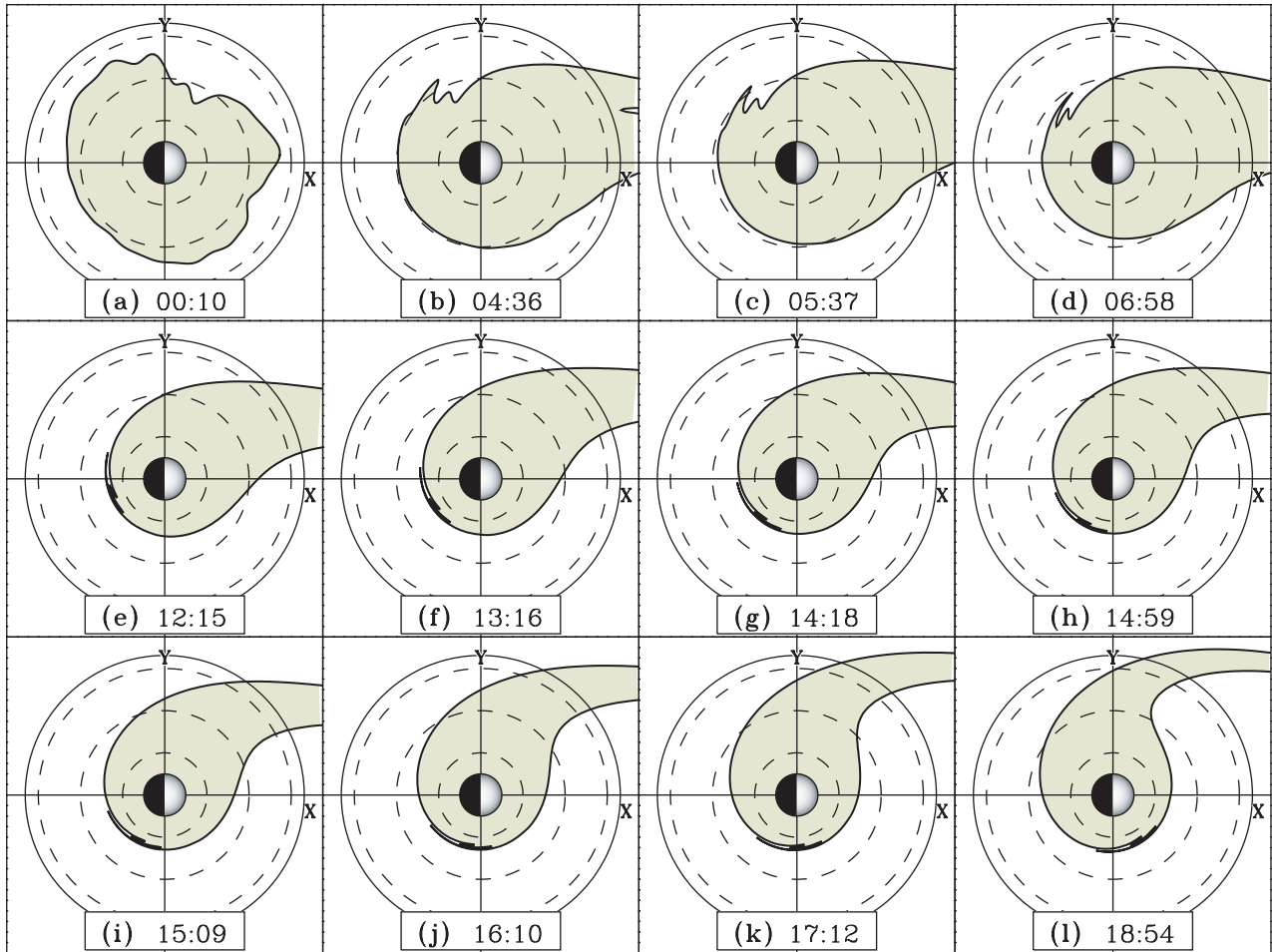
Plate 4. Plasmapause test particle (PTP) simulation of 18 June 2001 event, plotted in a format similar to that of Plate 1, with snapshots at the same times as panels a through l of Plate 1. In each plot, the plasmasphere is indicated by the green region surrounding the Earth. The simulation results indicate an erosion and plume development sequence that agrees with the EUV images on a global level, but there are important meso-scale and fine-scale differences, as discussed in the text.

(a) 00:10   (c) 05:37   (g) 14:18   (k) 17:12

Initial   Sunward Surge   Plume Narrowing   Plume Rotating
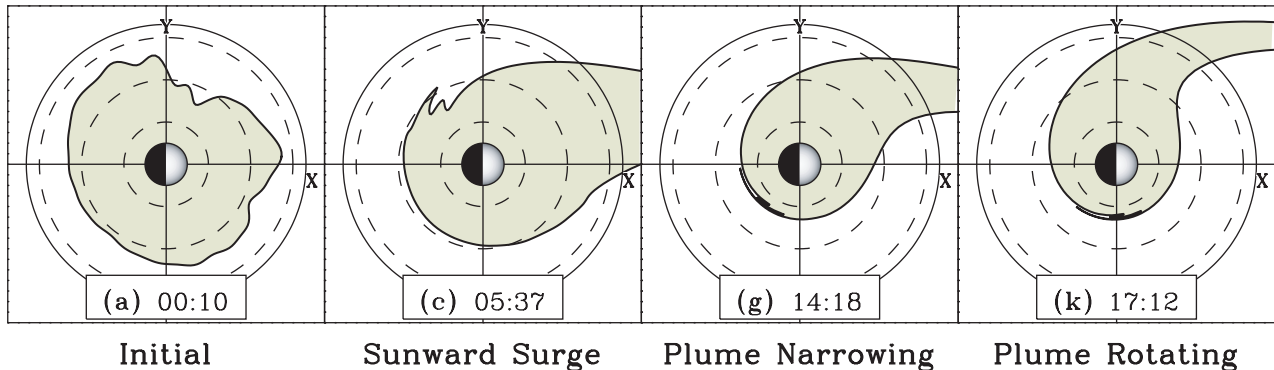
Plate 5. Four selected panels a, c, g, and k from Plate 4, each showing a PTP simulated plasmasphere. This figure should be directly compared with Plate 2. The phases of plume evolution from Plate 2 are evident in the simulation results (see text).
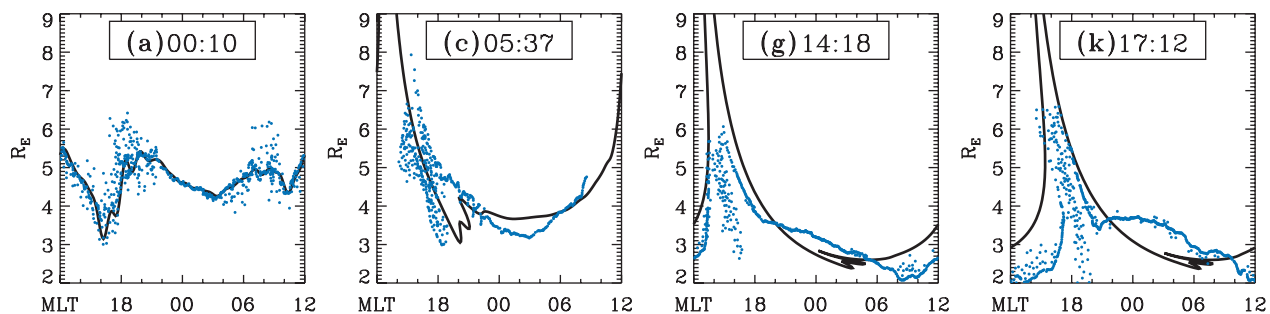
Plate 6. A more quantitative comparison between the EUV data of Plate 2 and the PTP simulation of Plate 5. In each of panels a, c, g, and k: blue circles plot the manually extracted plasmapause from EUV, and the solid black curve is the PTP simulated plasmapause. Although the zero-order global features are reproduced by the model, there are key differences, as discussed in the text.